AGU PUBLICATIONS

Paleoceanography

RESEARCH ARTICLE
10.1002/2015PA002918

Key Points:
- Diagenetic calcite influence on planktic stable isotopes
- Low-frequency response to insolation and paleogeography
- The Pliocene Nordic Seas were characterized by a succession of distinct climate phases

Correspondence to:
B. Risebrobakken,
bjorg.risebrobakken@uni.no

Citation:
Risebrobakken, B., C. Andersson, S. De Schepper, and E. L. McClymont (2016), Low-frequency Pliocene climate variability in the eastern Nordic Seas, *Paleoceanography*, *31*, 1154–1175, doi:10.1002/2015PA002918.

Received 17 DEC 2015
Accepted 12 JUL 2016
Accepted article online 22 AUG 2016
Published online 17 SEP 2016

Low-frequency Pliocene climate variability in the eastern Nordic Seas

Bjørg Risebrobakken[1], Carin Andersson[1], Stijn De Schepper[1], and Erin L. McClymont[2]

[1]Uni Research Climate, Bjerknes Centre for Climate Research, Bergen, Norway, [2]Department of Geography, Durham University, Durham, UK

Abstract The Pliocene (5.3–2.6 Ma) is often described as a relatively stable climatic period, with warm temperatures characterizing high latitudes. New suborbital resolved stable isotope records from Ocean Drilling Program Hole 642B in the eastern Nordic Seas document that the Pliocene was not a stable period characterized by one climate. Rather, seven distinct climate phases, each lasting between 150,000 and 400,000 years, are identified and characterized in the time interval 5.1–3.1 Ma. Four of the transitions between the defined climate phases occurred close to an eccentricity minimum and a minimum in amplitude of change for Northern Hemisphere summer insolation, while two occurred around an eccentricity maximum and a maximum in amplitude in insolation change. Hence, a low-frequency response of the Nordic Seas to insolation forcing is indicated. In addition, paleogeographic and related paleoceanographic changes, expansion of the Arctic sea ice cover, and onset of Northern Hemisphere glaciation were important factors behind the evolving Pliocene low-frequency variability in the eastern Nordic Seas. It is likely that the identified climate phases and transitions are important beyond the Nordic Seas, due to their association with changes to both insolation and paleogeography. However, a strong and variable degree of diagenetic calcite overgrowth is documented for the planktic foraminifera, especially influencing the planktic $\delta^{18}O$ results; the absolute values and amplitude of change cannot be taken at face value.

1. Introduction

The Pliocene (5.3–2.6 Ma) is characterized by an atmospheric CO_2 concentration of 350–450 ppm and global mean sea surface temperature (SST) 2–3°C higher than preindustrial [*Bartoli et al*., 2011; *Dowsett et al*., 2013; *Martínez-Botí et al*., 2015; *Seki et al*., 2010]. The configuration of the continents was similar to the present, although not all ocean gateways had reached the modern state [*Hill*, 2015]. The West Antarctic and Greenland ice sheets were substantially smaller, in line with global sea level estimates ranging from 10 to 40 m above present [*Raymo et al*., 2011]. At orbital timescales, the early Pliocene is characterized at a global scale by lower amplitude climate variability relative to the latest Pliocene and Quaternary [*Federov et al*., 2006; *Lisiecki and Raymo*, 2005], when Northern Hemisphere glaciation intensified. In the Nordic Seas, the effects of the intensification of the Northern Hemisphere glaciation are seen by a large increase in the deposition of ice-rafted debris between 3 and 2.6 Ma [*Fronval and Jansen*, 1996]. With the emergence of more data that cover parts of the Pliocene epoch at higher resolution, a more variable picture of Pliocene high-latitude climate has appeared at orbital and suborbital timescales, both on land [*Brigham-Grette et al*., 2013] and in the ocean [*Bachem et al*., 2016; *Bolton et al*., 2010; *Federov et al*., 2013; *Lawrence et al*., 2009].

The Nordic Seas encompass a complex region characterized by large horizontal and vertical temperature and salinity gradients related to the interaction between Atlantic and polar water masses [*Blindheim and Østerhus*, 2005; *Furevik and Nilsen*, 2005]. Due to processes contributing to "Arctic amplification," the high northern latitudes are expected to experience stronger warming than the low latitudes under a globally warmer climate [*Miller et al*., 2010], including during the Pliocene epoch. The Nordic Seas link the North Atlantic and Arctic Oceans, and the region is a dynamic part of the global oceans that is important for understanding the overturning circulation, poleward heat transport, and hence Arctic amplification. Despite the importance of the Nordic Seas region in governing large-scale climate, it is poorly characterized in Pliocene paleoceanography. Existing Pliocene data from the Nordic Seas indicate persistently warmer than present sea surface temperatures (SSTs) at the Iceland Plateau and the Yermak Plateau [*Bachem et al*., 2016; *De Schepper et al*., 2015; *Knies et al*., 2014a; *Robinson*, 2009; *Schreck et al*., 2013]. Early Pliocene palynomorphs and ostracods found in the Tjörnes sequence in Iceland indicate warmer than present conditions [*Cronin*, 1991; *Verhoeven et al*., 2011], while mollusc $\delta^{18}O$ indicate periods with temperatures comparable to modern (circa 4.7–4.4 Ma) and

warmer than modern (prior to circa 4.7 Ma) [*Buchardt and Símonarson*, 2003]. However, no suborbitally resolved records providing information on the long-term Pliocene paleoceanography of the Nordic Seas have so far been published.

Since the Pliocene is considered to be the closest past analogue to the predicted future warm climate when it comes to climatic boundary conditions [*Haywood et al*., 2011], and given the importance of the Nordic Seas region for understanding high-latitude responses to global warmth, we aim to investigate the climatic and oceanographic development of the eastern Nordic Seas during the Pliocene and to consider how the Pliocene climate and oceanography of the eastern Nordic Seas may differ from the present interglacial. As the new data here span most of the Pliocene epoch, we aim to investigate the potential linkages between the eastern Nordic Seas climatic and oceanographic development through the Pliocene with known changes in driving mechanisms and forcing, including paleogeography, Arctic sea ice cover, the onset or intensification of Northern Hemisphere glaciation, insolation, and atmospheric CO_2 concentrations. To achieve this aim, we present new suborbitally resolved planktic and benthic $\delta^{18}O$ and $\delta^{13}C$ records from Ocean Drilling Program (ODP) Hole 642B (Vøring Plateau). The focus is to reconstruct and determine the oceanographic changes that took place in the Nordic Seas over the Pliocene, and assess the causes behind the observed changes, by creating evidence of changing ocean properties at both the sea surface and at depth (~1300 m below the sea surface).

2. Present-Day Nordic Seas Oceanography

The Norwegian Atlantic Current (NwAC) brings warm and salty Atlantic water masses from the North Atlantic through the Nordic Seas toward the Arctic [*Orvik and Niiler*, 2002], while polar water is transported southward from the Arctic Ocean in the East Greenland Current (EGC) (Figure 1). The NwAC gradually loses its heat to the atmosphere and becomes denser as it moves northward. The Atlantic water (AW) is modified and becomes increasingly dense as it moves in the subsurface through the Return Atlantic Current (RAC), and through the Fram Strait and the Barents Sea into the Arctic Ocean, ultimately returning as distinct layers of the EGC. The RAC- and Fram Strait-derived water feeds the Denmark Strait overflow, while the water derived from the Barents Sea branch ultimately feeds the Iceland-Scotland overflow [*Mauritzen*, 1996]. The main currents are strongly steered by topography, and strong temperature and salinity gradients are set within the upper water column both in the N-S and E-W directions (Figure 1). At the Vøring Plateau the AW layer (7.0–9.5°C; 35.1–35.3 practical salinity unit (psu)) is 500–600 m thick [*Blindheim and Østerhus*, 2005; *Mauritzen*, 1996]. Between the AW and the deep bottom water (34.91 psu; $<$0.5°C; deeper than approximately 1100 m), Arctic Intermediate Water is seen as a salinity minimum zone (34.7–34.9 psu; $-$0.5–0.5°C) [*Blindheim and Østerhus*, 2005].

3. Material, Age Model, and Methods

Ocean Drilling Program Hole 642B was drilled during ODP Leg 104, at the Vøring Plateau in the eastern Nordic Seas (67°13.5′N, 2°55.7′E, 1286 m water depth) (Figure 1). We have investigated the Pliocene section of Hole 642B. We chose to investigate Site 642 since it is the only site from the Nordic Seas where foraminifera-based Pliocene records can be obtained; Nordic Seas Sites 907 and 643 are barren of foraminifera during the Pliocene due to dissolution [*Fronval and Jansen*, 1996], and Vøring Plateau Site 644 only recovers the last 3 Ma [*Shipboard Scientific Party*, 1987]. Therefore, the records presented here provide unique information for the Nordic Seas region through the Pliocene.

A hiatus was previously identified near the 104–642B–8H/9H core section boundary, corresponding to the younger part of the Pliocene [*Bleil*, 1989; *Spiegler and Jansen*, 1989]. We have identified that the core is barren of foraminifera between 88.43 and 83.61 m below seafloor (mbsf). Our study thus focuses on core sections 10H6 through 9H1, between 83.61 and 66.94 mbsf or between 5.05 and 3.14 Ma according to our age model. The core is sampled every 1 cm from 9H1, 53–54 cm through 9H2, 130–131 cm (233 samples) and at least every 5 cm from 9H2, and 130–131 cm to 10H6, 20–21 cm (473 samples). Due to previous sampling of the core, no material was available for analysis in the intervals 9H3, 120 to 150 cm, 10H4, 135 to 150 cm, and 9H2, 0 to 10 cm.

Our age model for the Pliocene section of Hole 642B is primarily based on the magnetic stratigraphy of *Bleil* [1989] with ages updated to ATNTS2012 [*Hilgen et al*., 2012] and further constrained by correlating our five-point running mean benthic $\delta^{18}O$ record with the global LR04 benthic $\delta^{18}O$ stack [*Lisiecki and Raymo*,

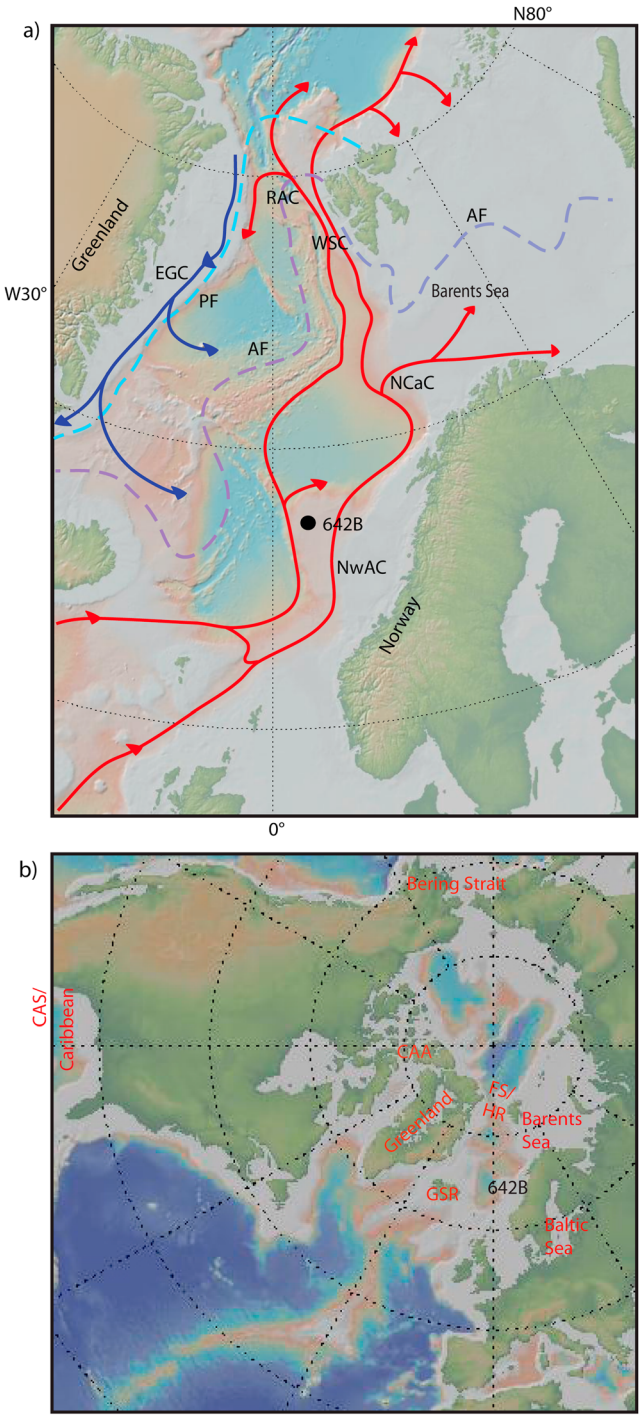

Figure 1. (a) Present-day oceanographic features of the Nordic Seas and the location of ODP Hole 642B. NwAC: Norwegian Atlantic Current. NCaC: North Cape Current. EGC: East Greenland Current. WSC: West Spitsbergen Current. RAC: Return Atlantic Current. PF: polar front. AF: Arctic Front. (b) Locations of discussed gateways are indicated. CAS: Central American Seaway. CAA: Canadian Arctic Archipelago. GSR: Greenland Scotland Ridge. FS/HR: Fram Strait/Hovgård Ridge.

2005] (Figures 2 and 3 and Table 1). A five-point running mean of the benthic $\delta^{18}O$ record was used to avoid putting emphasis on potential local signals when comparing to the global stack. More specifically, we have used eight extra tie points within the Gilbert Chron, based on the benthic oxygen isotopes. Furthermore, the isotopes fully constrain our chronology from marine isotope stage (MIS) MG7/MG8 (4.147 Ma) to KM3/KM2 (3.136 Ma) (Figure 3 and Table 1). The uncertainty related to the LR04 stack is considered to be 40 ky between 5 and 4 Ma and 15 ky between 4 and 3 Ma [*Lisiecki and Raymo*, 2005]. The uncertainty related to the timing of the magnetic reversals is argued to be half the age difference between the two adjacent samples that record the reversal [*De Schepper and Head*, 2008]. In the case of Hole 642B this will be less than 5 ky. Biostratigraphical information from dinoflagellate cysts supports our updated age model [*De Schepper et al.*, 2015].

Comparing our Hole 642B benthic $\delta^{18}O$ with the LR04 stack, it is clear that even though the pattern of variability and amplitude of change is similar through large parts of the record (Figure 3), absolute benthic $\delta^{18}O$ values are higher in our Nordic Seas record than in LR04, and the long-term trends also differ (Figure 2). The pattern of variability is most different in the early Pliocene, where we have the lowest sampling resolution. For this part of the record we build the chronology solely on the identified paleomagnetic reversals, since the different frequency of $\delta^{18}O$ signals between the Hole 642B and LR04 could reflect sampling resolution and/or local signatures over our new data, both of which could lead to inappropriate age assignment if we attempted to tune the two data sets.

Based on our new chronological framework, the sedimentation rates are between 2 and 20 cm/ky (Figure 2). Sedimentation rates at the Vøring Plateau are known to show large changes at specific sites with changing

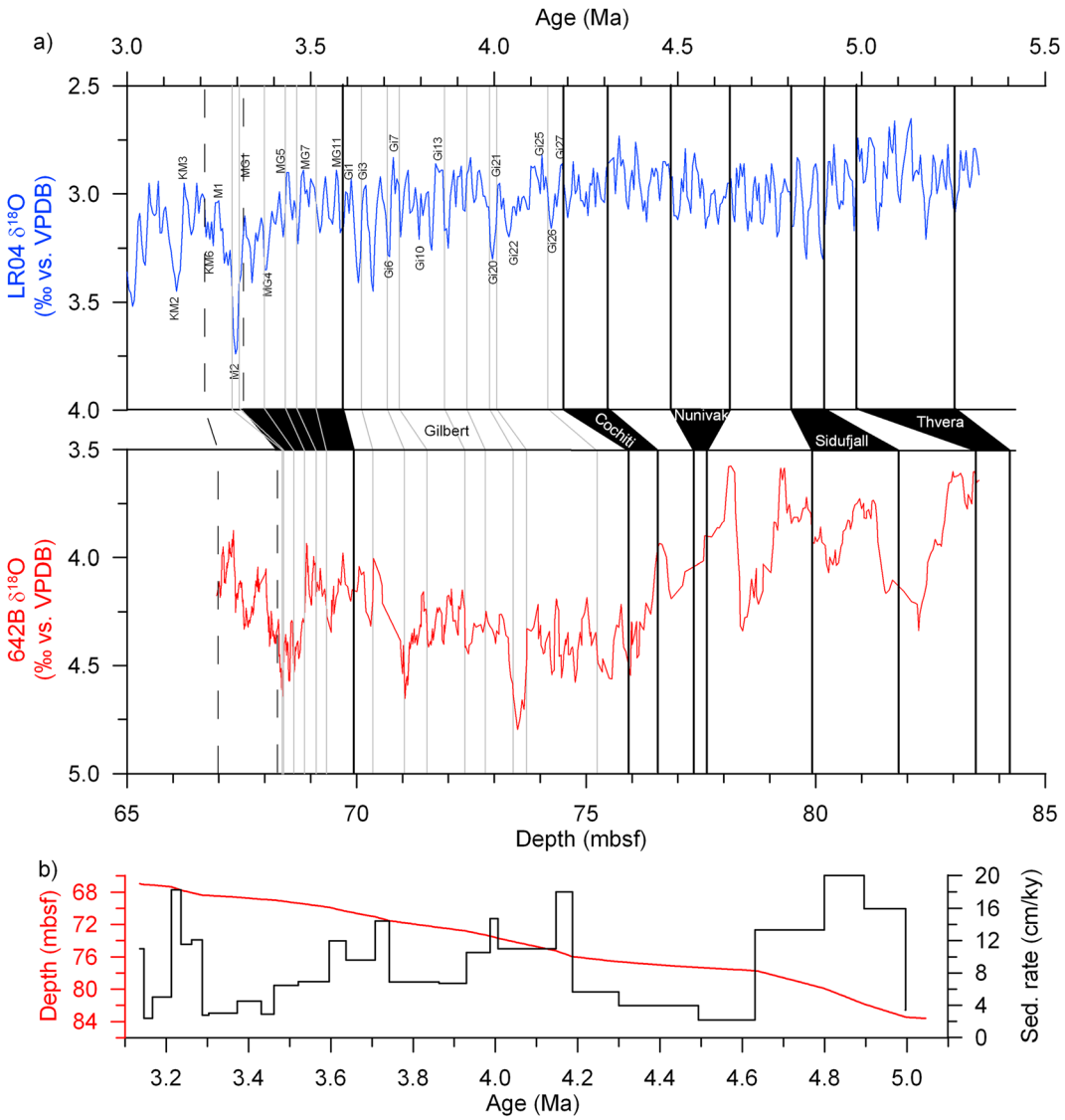

Figure 2. (a) The five-point running mean of *C. teretis* $\delta^{18}O$ from Hole 642B versus depth (red) and the global LR04 benthic $\delta^{18}O$ stack versus age (blue) [*Lisiecki and Raymo*, 2005]. Black lines show the corresponding locations of the magnetic reversals throughout the Pliocene, and the magnetic periods are indicated in black and white between the panels. Dashed black lines indicate reversals not used as a tie point when calculating the final ages, corresponding to an interval where the age model is based solely on correlating the $\delta^{18}O_{C.t.}$ (five-point running mean) to the LR04 stack. Tie points for this interval are indicated in Figure 3. Grey lines shown between 3.3 and 4.2 Ma correspond to further tie points used based on the correlation between Hole 642B $\delta^{18}O_{C.t.}$ and the LR04 stack. Indicated marine isotope stages refer to stages as defined in *Lisiecki and Raymo* [2005]. (b) The new age model for Hole 642B and corresponding sedimentation rates.

climate conditions. Some sites experience enhanced sedimentation during interglacials (glacials), and reduced during glacials (interglacials) [*Dokken and Jansen*, 1999; *Dreger*, 1999; *Risebrobakken et al.*, 2003], dependent on the changing strengths of local bottom water currents under different climate regimes and how that influences the location of the main deposition centers. The changes in sedimentation rates recorded in Hole 642B are smaller than the changes known to take place between late Quaternary glacials and interglacials in the same area, as expected before the onset of large-scale Northern Hemisphere glaciations. Hence, the changes in sedimentation rates observed in Hole 642B are considered realistic for the area and time interval investigated.

Marine isotope stage M2 is the earliest well-defined Pliocene glacial period seen in the LR04 stack [*Lisiecki and Raymo*, 2005] and through well-defined ice-rafted debris (IRD) peaks at the Iceland and Yermak Plateaus

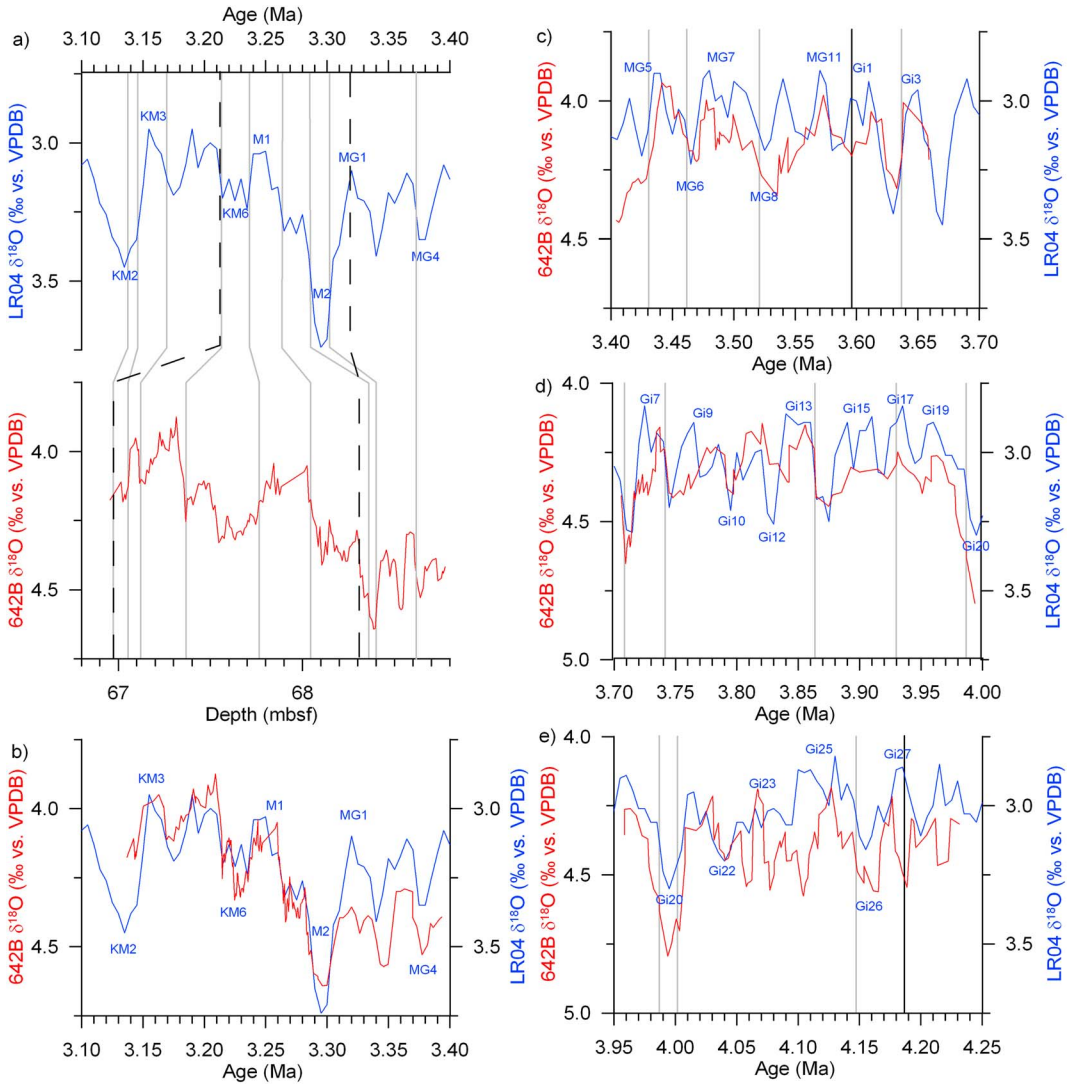

Figure 3. Zooming in on parts of the record where the five-point running mean $\delta^{18}O_{C.t.}$ and the LR04 stack [*Lisiecki and Raymo*, 2005] have been used to constrain the chronology, alone or in combination with the magnetic reversals. Hole 642B $\delta^{18}O_{C.t.}$ is shown in red, while LR04 is shown in blue in all panels. Indicated marine isotope stages refer to stages as defined in *Lisiecki and Raymo* [2005]. The grey lines correspond to the tie points that were defined from correlating the $\delta^{18}O_{C.t.}$ and the LR04 and represent the tie points used for calculating the age model. The dashed black lines represent the magnetic reversals not used when establishing the new Hole 642B chronology. Black lines represent magnetic reversals used as tie points when establishing the new Hole 642B chronology. (a) The correlation between Hole 642B and LR04 between 3.40 and 3.10 Ma. (b) The correlation between Hole 642B and LR04 from 3.70 and 3.40 Ma. (c) The correlation between Hole 642B and LR04 between 4.00 and 3.70 Ma. (d) The correlation between Hole 642B and LR04 between 3.95 and 4.25 Ma. Details on exact ages and corresponding mbsf depths for all tie points are given in Table 1.

[*Jansen et al*., 2000; *Knies et al*., 2014b]. MIS M2 is also a well-pronounced glacial in the North Atlantic [*De Schepper et al*., 2013]. At Hole 642B, the benthic $\delta^{18}O$ signal is no heavier than at several other occasions earlier in the Pliocene and no IRD is seen during MIS M2 [*Jansen et al*., 1990]. One possibility is that this reflects a minor hiatus over the most extreme part of MIS M2 or alternatively that M2 was a less extreme event locally than expressed in other regions. Another possibility to be considered is that overgrowth of diagenetic calcite may have made the older glacials, e.g., MIS Gi20 and Gi6 (Figure 2), appear artificially heavy and thus reduced the amplitude of the signal for MIS M2 (see discussion in section 5.1).

Planktic and benthic $\delta^{18}O$ and $\delta^{13}C$ were measured in Bergen, using Finnigan MAT 252 and MAT 253 mass spectrometers equipped with an automatic preparation line ("Kiel device"). All foraminifera were picked from the $>150\,\mu m$ fraction then crushed and cleaned with methanol, using an ultrasonic bath, before being

AGU Paleoceanography

10.1002/2015PA002918

Table 1. Tie Points Used to Establish the Updated Age Model of 642B [a]

Chron/Subchron [*Bleil*, 1989]	Chron/Subchron (ATNTA2012)	Comment	B85 Ma[b]	CK92Ma[c]	LR04 Ma[d]	ATNTA 2004/2012 Ma[e]	Sample	Upper Depth (m bsf)	Sample	Lower Depth (m bsf)	Middepth (m bsf)	642B Tie Points (m bsf)	Tie Points (Ma)
		KM2/KM3-top			3.136		9H1, 54-55					66.95	3.136
		KM2/KM3			3.146		9H1, 65-66					67.06	3.146
		KM3/KM4			3.167		9H1, 70-71					67.11	3.167
		KM5/KM6			3.213		9H1, 93-94					67.34	3.213
		KM6/M1			3.236		9H1, 135-136					67.76	3.236
		M1/M2			3.262		9H2, 15-16					68.06	3.262
		M1/M2			3.287							68.37	3.287
		M2/MG1			3.303		9H2, 50-51					68.41	3.303
C2AN-2/C2AR-2	C2An.2n/C2An.2r	Top Mammoth	3.08	3.221	3.210	3.207	9H1, 41	66.81	9H1, 71	67.11	66.96		
A2AR-2/C2AN-3	C2An.2r/C2An.3n	Base Mammoth	3.18	3.325	3.319	3.330	9H2, 11	68.01	9H2, 41	68.31	68.16		
		MG3/MG4			3.373		9H2, 71-72					68.62	3.373
		MG5			3.431		9H2, 97-98					68.88	3.431
		MG5/MG6			3.462		9H2, 106-107					69.97	3.462
		MG7/MG8			3.521		9H2, 144-146					69.34	3.521
C2AN-3/C2AR-3	C2An.3n/C2r	Top Gilbert	3.40	3.553	3.588	3.596	9H3, 47	69.87	9H3, 71	70.11	69.99	69.87	3.596
		Gi2/Gi3			3.637		9H3, 95-96					70.36	3.637
		Gi5/Gi6			3.708							71.04	3.708
		Gi7/Gi8			3.742							71.53	3.742
		Gi13/Gi14			3.863		9H4, 145-146					72.36	3.863
		Gi16/Gi17			3.930							72.81	3.930
		Gi19/Gi20			3.987		9H5, 100-101					73.41	3.987
		Gi20/Gi21			4.006							73.69	4.006
		Gi25/Gi26			4.147							75.24	4.147
C2AR-3/C3N-1	C2Ar/C3n.1n	Top Cochiti	3.88	4.033	4.187	4.187	9H7, 56	75.96	10H1, 9	75.99	75.98	75.96	4.187
C3N-1/C3-1	C3n.1n/C3n.1r	Base Cochiti	3.97	4.134	4.306	4.300	10H1, 70	76.60	10H1, 101	76.91	76.76	76.60	4.300
C3R-1/C3N-2	C3n.1r/C3n.2n	Top Nunivak	4.10	4.265	4.478	4.493	10H1, 130	77.20	10H2, 11	77.51	77.36	77.36	4.493
C3N-2/C3R-2	C3n.2n/C3n.2r	Base Nunivak	4.24	4.432	4.642	4.631	10H2, 11	77.51	10H2, 41	77.81	77.66	77.60	4.631
C3R-2/C3N-3	C3n.2r/C3n.3n	Top Sidufjall	4.40	4.611	4.807	4.799	10H3, 71	79.61	10H3, 100	79.90	79.76	79.90	4.799
C3N-3/C3R-3	C3n.3n/C3N.3r	Base Sidufjall	4.47	4.694	4.898	4.896	10H4, 126	81.66	10H5, 11	82.01	81.84	81.84	4.896
C3R-3/C3N-4	C3N.3r/C3n.4n	Top Thvera	4.57	4.812	4.989	4.997	10H5, 130	83.2	10H6, 10	83.5	83.35	83.45	4.997
C3N-4/C3R-4(?)	C3n.4n/C3r	Base Thvera	4.77	5.046	5.254	5.235	10H6, 71	84.11	10H6, 100	84.4	84.255	84.255	5.235
C3R-4(?)/(C3A)C3AN-1	C3R/C3An.1n		5.35	5.705		6.033	12H2, 71	97.11	10H2, 101	97.41	97.26	97.26	6.033

[a]The tie points are either based on magnetic reversals, updated to ATNTA2012, or on the correlation between our five-point running mean $\delta^{18}O_b$ and the LR04 global benthic $\delta^{18}O$ stack [*Lisiecki and Raymo*, 2005].
[b]*Berggren et al.* [1985], used for the *Bleil* [1989] 642B age model.
[c]*Cande and Kent* [1995], used for the *Fronval and Jansen* [1996] 642B age model.
[d]*Lisiecki and Raymo* [2005].
[e]*Hilgen et al.* [2012].

Table 2. Holocene Mean (±1σ), Maximum and Minimum Stable Isotope Values as Measured for *G. bulloides* and *C. teretis*, and Mean Weight of the *G. bulloides* Specimens Measured for Holocene Stable Isotopes From the Vøring Plateau Core MD95-2011 (66°58.19 N, 7°38.36E, 1048 m Water Depth) [*Dei Tos*, 2011; *Risebrobakken et al*., 2011; Risebrobakken, Unpublished Data]

	$\delta^{18}O_{G.b.}$ ‰ Versus VPDB	$\delta^{13}C_{G.b.}$ ‰ Versus VPDB	$\delta^{18}O_{C.t.}$ ‰ Versus VPDB	$\delta^{13}C_{C.t.}$ ‰ Versus VPDB	$\Delta\delta^{13}C_{G.b.\text{-}C.t.}$ ‰ Versus VPDB	G.b. Weight (μm)
Holocene mean ±1σ (0–9 ka)	1.68 ± 0.28	−0.34 ± 0.33	4.10 ± 0.23	−0.59 ± 0.21	−0.23 ± 0.31	10 ± 2
Holocene maximum (0–9 ka)	2.24	0.35	4.76	0.12	0.43	18
Holocene minimum (0–9 ka)	0.95	−1.68	3.32	−1.58	−1.03	4

measured. The measurements were undertaken on 1–8 specimens of *Globigerina bulloides* ($\delta^{18}O_{G.b.}$ and $\delta^{13}C_{G.b.}$) and 1–10 specimens of *Cassidulina teretis* ($\delta^{18}O_{C.t.}$ and $\delta^{13}C_{C.t.}$). Of the 1041 measurements undertaken for this study, 5 were analyzed on single specimens. The Pliocene planktic foraminifera fauna in Hole 642B is dominated by *Neogloboquadrina atlantica*, a species that is extinct today [*Poore and Berggren*, 1975]. Planktic isotope measurements are therefore undertaken on *Globigerina bulloides* since it is the planktic species that we know from the present day and which is also available in most samples. *Cassidulina teretis* is a commonly used benthic species for isotope analyses in the Nordic Seas and is present through the investigated time interval. Furthermore, we have Holocene reference data available from the study area for both *G. bulloides* and *C. teretis* (Table 2).

The analytical uncertainty is ±0.08‰ and ±0.03‰ for oxygen and carbon isotopes, respectively. All results are reported in ‰ versus Vienna Peedee belemnite (VPDB), using National Bureau of Standards (NBS) 19 or NBS 18, in combination with the lab internal standard CM12. Our $\delta^{18}O_{C.t.}$ and $\delta^{13}C_{C.t.}$ results are combined with the lower resolution Pliocene $\delta^{18}O_{C.t.}$ and $\delta^{13}C_{C.t.}$ measurements presented by *Jansen et al*. [1990]. *Cassidulina teretis* calcifies close to equilibrium [*Jansen et al*., 1988]. Therefore, no correction for departure from isotopic equilibrium is applied for $\delta^{18}O_{C.t.}$ The stable isotope records are smoothed using a five-point running mean average, to better visualize the long-term trends that are the focus of this study.

The resulting measurements integrate information on a time span longer than any instrumental record, and core top measurements are not representative of the range of variability that exists within a warm climate. To include information on the range of variability occurring within a warm interglacial period, we compare our Pliocene isotope records to Holocene (0–9 ka) reference values from isotope records measured on the same species in Vøring Plateau core MD95-2011 (66°58.19 N, 7°38.36E, 1048 m water depth) [*Dei Tos*, 2011; *Risebrobakken et al*., 2011; B. Risebrobakken, unpublished carbon isotopes data, 2016] (Table 2).

An ice volume correction is applied to the $\delta^{18}O$ time series so that the records are influenced by the same factors when comparing the Pliocene and Holocene. The global sea level is estimated to have been 10–40 m higher than today at about 3 Ma [*Raymo et al*., 2011], largely due to the reduced size of the West Antarctic and Greenland ice sheets. The exact ice volume changes through the Pliocene are, however, not known. The global benthic $\delta^{18}O$ stack, LR04 [*Lisiecki and Raymo*, 2005], gives a first-order estimate of ice volume changes, even though a smaller temperature component is also present. We follow the approach of *Miller et al*. [2012], calculating the residual between all LR04 Pliocene $\delta^{18}O$ values and the modern-day $\delta^{18}O$ of LR04; ice volume is assumed to be responsible for 67%, and temperature 33%, of the residual $\delta^{18}O$ signal, consistent with the Pleistocene glacial-interglacial changes [*Fairbanks*, 1989]. We also calculated the end-member assumptions of 50:50 and 80:20 ice volume:temperature to illustrate the likely error ranges associated with subtracting a ice volume contribution to our benthic $\delta^{18}O$ data [*Miller et al*., 2012]. The calculated 67% of the residual LR04 $\delta^{18}O$ (and the 80% and 50% end-members) are used to correct the Hole 642B $\delta^{18}O_{G.b.}$ and $\delta^{18}O_{C.t.}$ for the difference in ice volume between the present and the Pliocene, having first ensured that both data sets were on the same timescale (Table 1). Correcting for the mostly smaller Pliocene global ice volume leads to slight increases in the $\delta^{18}O_{G.b.}$ and $\delta^{18}O_{C.t.}$ values (Figure 4). The corrected records represent a mixed temperature and salinity signal, and hence density, of the respective water masses. In sections 4 and 5 we will focus on these ice volume-corrected records.

4. Results

The following general characteristics are identified based on the smoothed Hole 642B $\delta^{18}O$ and $\delta^{13}C$ (Figure 4):

1. The Pliocene climate was not stable in the Nordic Seas.

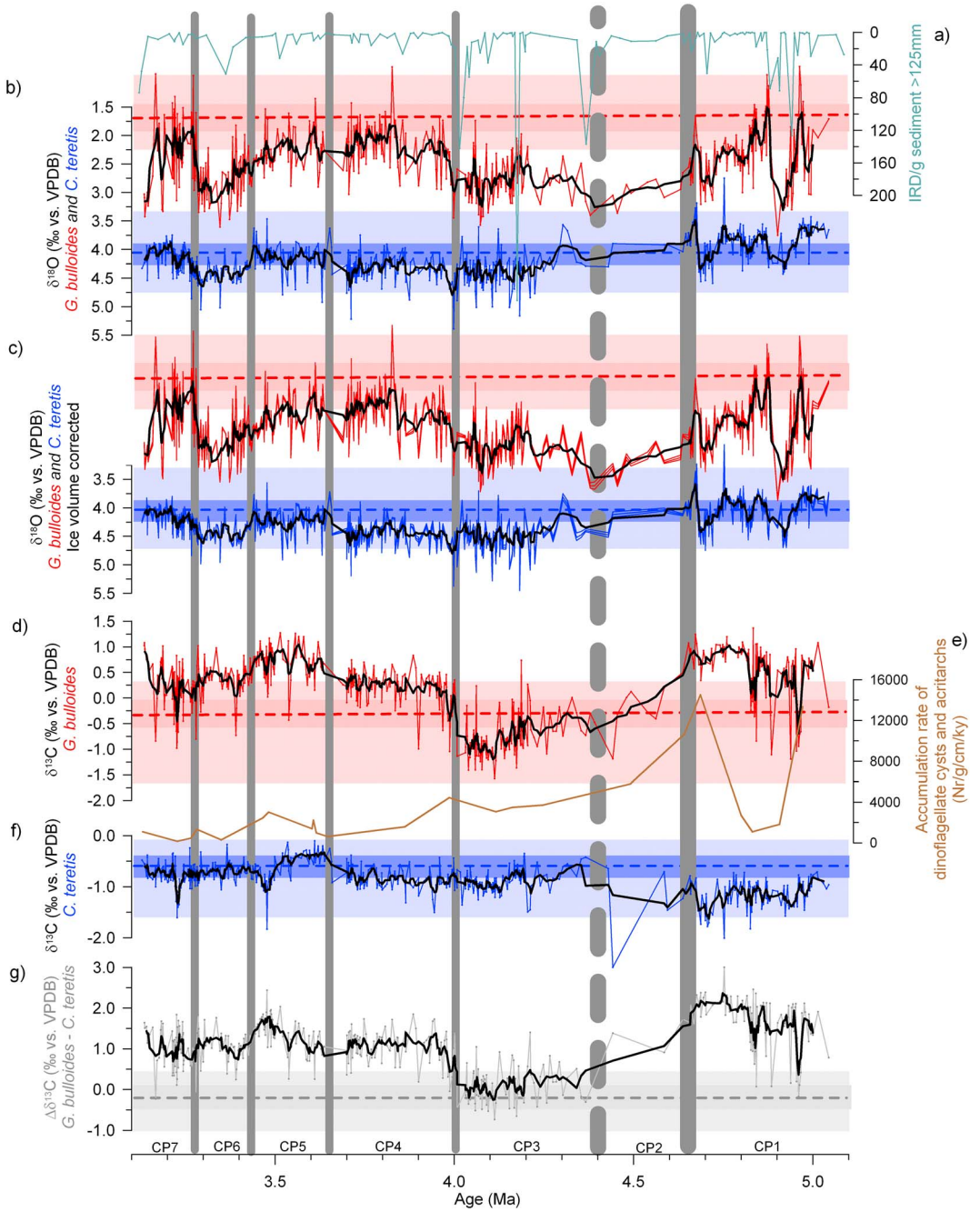

Figure 4. (a) Ice-rafted debris/g sediment (>125 μm) from Hole 642B [*Jansen et al.*, 1990]. (b) $\delta^{18}O_{C.t.}$ (blue) and $\delta^{18}O_{G.b.}$ (red). (c) Ice volume-corrected $\delta^{18}O_{C.t.}$ (blue) and $\delta^{18}O_{G.b.}$ (red). The different lines represent the difference between assuming that 80, 67, or 50% of the residual LR04 signal represents a response to ice volume changes. $\delta^{18}O_{G.b.}$ is shown without reference to absolute values to emphasize that these cannot be trusted due to the influence of diagenetic calcite. (d) $\delta^{13}C_{G.b.}$ (e) Accumulation rates of acritarchs and dinoflagellate cysts (based on *De Schepper et al.* [2015]). (f) $\delta^{13}C_{C.t.}$. (g) $\Delta\delta^{13}C_{G.b.-C.t.}$. For all isotope records, the thick black lines represent the five-point smoothed records. Horizontal dashed lines represent the Holocene mean (last 9 ka) (Table 2 and section 3), the darker bands indicate the ±1 standard deviation range for the Holocene mean value, while the lighter bands indicate the maximum and minimum values recorded through the last 9 ka. Vertical grey lines indicate the timing of the transitions between the climate phases. The stippled vertical line indicates the larger uncertainty related to the transition between CP1 and CP2. The thickness of the grey lines reflects the age uncertainties for different Pliocene intervals as indicated by *Lisiecki and Raymo* [2005], 30 ky between 5 and 4 Ma and 15 ky between 4 and 3 Ma.

2. $\delta^{18}O_{C.t.}$ and $\delta^{13}C_{C.t.}$ vary within the range of Holocene variability of the same proxy, but through large parts of the Pliocene, the $\delta^{18}O_{C.t.}$ values are higher than the Holocene mean, while the $\delta^{13}C_{C.t.}$ values are lower than the Holocene mean.
3. The $\delta^{18}O_{G.b.}$ and $\delta^{13}C_{G.b.}$ records indicate a larger amplitude of change in the Pliocene than the benthic records. The $\delta^{18}O_{G.b.}$ data have higher values than at any time during the Holocene on several occasions and values that are unexpected for a globally warmer time interval. $\delta^{13}C_{G.b.}$ is higher than the Holocene mean and often higher than the highest Holocene value, with the exception of the 4.5–4 Ma interval.
4. The difference between planktic and benthic carbon isotopes, $\Delta\delta^{13}C_{G.b.\text{-}C.t.}$, is only within the range of Holocene values between 4.4 and 4.0 Ma; at all other times the $\Delta\delta^{13}C_{G.b.\text{-}C.t.}$ is higher than the highest Holocene values.

Based on the combined stable isotope records, excluding $\delta^{18}O_{G.b.}$, we identify seven climate phases (CPs) with different character (Figure 4). In section 5.1 we discuss the potential impact of diagenetic calcite on the stable isotope records and especially on the $\delta^{18}O_{G.b.}$ record.

During the first climate phase, CP1 (5.05–4.65 Ma), rather large and simultaneous changes are recorded in both $\delta^{18}O_{C.t.}$ and $\delta^{18}O_{G.b.}$. The $\delta^{18}O_{C.t.}$ record oscillates around the Holocene mean (Figure 4). The $\delta^{13}C_{G.b.}$ is typically higher than the Holocene maximum, while $\delta^{13}C_{C.t.}$ is lower than the Holocene mean, causing the highest recorded Pliocene $\Delta\delta^{13}C_{G.b.\text{-}C.t.}$.

When entering the second climate phase, CP2 (4.65–4.4 Ma), the sediment becomes almost barren of foraminifera. Very few measurements are available, and the climatic and oceanographic conditions of this interval cannot be well defined (Figure 4). CP2 is, however, defined as a specific phase due to the low numbers of foraminifera in the sediment, which distinguishes it from the previous and following CP. Furthermore, the ice-rafted debris (IRD) record from the same core shows that CP2 is marked by very little variability [*Jansen et al.*, 1990], hence supporting the interpretation of this interval as different from CP1 and CP3 (Figure 4). Through CP2, a gradual increase in $\delta^{18}O_{C.t.}$, $\delta^{18}O_{G.b.}$, and $\delta^{13}C_{C.t.}$ is indicated, while $\delta^{13}C_{G.b.}$ indicates a gradual decrease.

The onset of the third climate phase, CP3 (4.4–4.0 Ma), is defined by the renewed presence of foraminifera in high enough numbers to sustain more regular stable isotope measurements and a return to large peaks in IRD (Figure 4). However, the onset of CP3 is the least well defined of the detected climate phases. Within CP3, both $\delta^{18}O_{G.b.}$ and $\delta^{18}O_{C.t.}$ are heavier than during CP1. The most enriched Pliocene $\delta^{18}O_{C.t.}$ values are recorded during this interval and lie close to the Holocene maximum. A gradual decrease of $\delta^{13}C_{G.b.}$ is recorded during CP3, from -0.3‰ to -1.2‰. All CP3 $\delta^{13}C_{G.b.}$ values are lower than the Holocene mean and, hence, lower than at any other point in our Pliocene record. The $\delta^{13}C_{C.t.}$ is more stable than the $\delta^{13}C_{G.b.}$ and consistently at a higher level than during CP1. This is the only interval when $\Delta\delta^{13}C_{G.b.\text{-}C.t.}$ are close to Holocene values.

The transition into the fourth climate phase, CP4 (4.0–3.65 Ma), is delineated by the rapid, strong increase in $\delta^{13}C_{G.b.}$. Following the abrupt increase, $\delta^{13}C_{G.b.}$ stabilizes at a level similar to the Holocene maximum. The transition also corresponds with a decrease in $\delta^{18}O_{G.b.}$ and a decrease in the amount of IRD deposited (Figure 4). Both $\delta^{18}O_{C.t.}$ and $\delta^{13}C_{C.t.}$ are maintained at the same level as in CP3, while a stepwise increase is indicated for $\delta^{18}O_{G.b.}$ in the middle of CP4. The $\Delta\delta^{13}C_{G.b.\text{-}C.t.}$ is higher than recorded at any point during the Holocene.

During the fifth climate phase, CP5 (3.65–3.42 Ma), $\delta^{13}C_{C.t.}$ and $\delta^{13}C_{G.b.}$ increase while $\delta^{18}O_{C.t.}$ decreases relative to the CP4 level (Figure 4). The highest Pliocene $\delta^{13}C_{C.t.}$ values are recorded during CP5, while $\delta^{13}C_{G.b.}$ values are similar to CP1. The $\delta^{18}O_{C.t.}$ values are close to the Holocene mean. $\delta^{18}O_{G.b.}$ changes of up to 0.5‰ are superimposed on an increasing trend throughout CP5, in contrast to the more stable $\delta^{18}O_{C.t.}$ record. The $\Delta\delta^{13}C_{G.b.\text{-}C.t.}$ values are higher than in CP4.

The onset of the sixth climate phase, CP6 (3.42–3.285 Ma), is defined by an increase in $\delta^{18}O_{C.t.}$ and a decrease in $\delta^{13}C_{G.b.}$ (Figure 4). Throughout CP6, the $\delta^{18}O_{C.t.}$ is sustained at high values, comparable to CP3 and CP4, while the $\delta^{13}C_{G.b.}$ record shows values comparable to CP4. The $\delta^{18}O_{C.t.}$ record stabilizes at values close to the Holocene mean, for the first time in the Pliocene record. A continued increasing trend is indicated for $\delta^{18}O_{G.b.}$.

The end of CP6 and the start of the seventh climate phase, CP7 (3.30–3.14 Ma), is defined by a sharp increase in $\delta^{18}O_{C.t.}$ and $\delta^{18}O_{G.b.}$ and a slight decrease in $\delta^{13}C_{G.b.}$ (Figure 4). The $\delta^{18}O_{C.t.}$ record stabilizes at values comparable to the Holocene mean, and the $\delta^{13}C_{G.b.}$ record stays at close to Holocene values, as during CP6.

5. Discussion

5.1. Influence of Secondary Processes on the Stable Isotope Records

As noted in section 4, the Pliocene $\delta^{18}O_{G.b.}$ data from Hole 642B are consistently higher than Holocene mean values. Since the Pliocene is considered to be warmer than present globally [*Dowsett et al*., 2013], this is an unexpected result, as it would suggest a colder Pliocene Nordic Seas region than at present. The foraminifera were seemingly well preserved when picking them under the stereomicroscope for isotope measurements. However, due to the unexpected results, we have investigated whether secondary processes may have influenced the $\delta^{18}O_{G.b.}$ data. Specifically, we have investigated whether the foraminifera have been influenced by diagenetic calcite. Pliocene SST estimates based on planktic $\delta^{18}O$ occasionally indicate colder SSTs than present, in contrast with SST estimates from other proxies and model runs that indicate higher than present temperatures [*Williams et al*., 2005]. It is suggested that these seemingly cold temperatures resulted from diagenetic calcite formed in cool seafloor sediment pore waters [*Williams et al*., 2005]. Adding diagenetic calcite with characteristics of the much colder seafloor sediment pore water after deposition will increase the $\delta^{18}O$ of the planktic foraminifera shells [*Kozdon et al*., 2013] and so may explain the unusually high $\delta^{18}O_{G.b.}$ results we have presented here. To consider the evidence for this process at Site 642B, we have examined both scanning electron microscope (SEM) images for selected samples and documented shell weight changes throughout the Pliocene.

5.1.1. Documenting an Influence of Secondary Processes on $\delta^{18}O_{G.b.}$

Scanning electron microscope pictures were taken of *G. bulloides* specimens which represent different extremes in the $\delta^{18}O_{G.b.}$ record. The SEM pictures show that none of the investigated specimens can be considered pristine, and the degree of overgrowth is profound for several of the specimens, e.g., pictures 3, 6, 7, and 9, related to CP1, CP4, CP5, and CP7 (Figure 5). Although the SEM pictures only represent single specimens from the different climate extremes, they show that the $\delta^{18}O_{G.b.}$ record has very likely been influenced by added diagenetic calcite. The absolute $\delta^{18}O_{G.b.}$ values should therefore not be trusted. The SEM pictures also show that the influence of diagenetic calcite has varied through time, rather than being stable or getting gradually worse with increasing sample age. Therefore, the absolute amplitude of change seen in the $\delta^{18}O_{G.b.}$ record should also be questioned, since some of the observed variability could reflect differing degrees of planktonic foraminifera diagenesis.

We also examined shell weight changes for the measured *G. bulloides* specimens for evidence of diagenesis. In Hole 642B, we do not have enough specimens in each sample for a statistically sound shell weight analysis [e.g., *de Villiers*, 2003]; however, the total sample weight and number of specimens used for each isotope measurement provide a rough estimate. This *G. bulloides* shell weight estimate also shows distinct changes through time (Figure 5). Several of the larger changes in shell weight occur at the same time as the transitions between defined CPs, e.g., the CP1/CP2, CP3/CP4, and CP5/CP6 transitions. The heaviest shell weights are seen during CP1 and CP5 where severe overgrowth of diagenetic calcite is shown by the SEM pictures 3 and 7 (Figure 5), indicating that the high shell weight might be linked to the degree of added diagenetic calcite to the foraminifera shell. Severe overgrowth is, however, also indicated by SEM pictures 6 and 9, during CP4 and CP7, when rather low shell weights are registered. Hence, for Hole 642B the relationship between shell weight and degree of diagenetic overgrowth as indicated by the SEM pictures is not constant, but it is likely that heavy shell weights indicates enhanced overgrowth.

Furthermore, the isotope composition of foraminifera can also be influenced by the size of the measured specimens [*Ezard et al*., 2015]. Since the measurements have been undertaken on specimens $>150\,\mu m$, the $\delta^{18}O_{G.b.}$ record might also be influenced by size-dependent effects. In other words, test size might be a common forcing factor when shell weight and $\delta^{18}O_{G.b.}$ covary. A high degree of scatter is, however, observed for *G. bulloides* oxygen isotope measurements, in general, independent of size [*Ezard et al*., 2015], making it hard to infer how size-specific effects might have influenced our results.

5.1.2. Can the $\delta^{18}O_{G.b.}$ Record Still Provide Information on Past Climate?

We have shown that secondary processes influence the $\delta^{18}O_{G.b.}$ signal at Hole 642B, and it should therefore be questioned whether the site holds any trustworthy climate information. The long-term trend of the $\delta^{18}O_{G.b.}$ record shows resemblance with the long-term trends of $\delta^{18}O_{C.t.}$, $\delta^{13}C_{G.b.}$, and $\delta^{13}C_{C.t.}$ from Hole 642B as well as main features of the IRD record of *Jansen et al*. [1990] from the same Hole (Figure 4). Clear similarities are also seen between Hole 642B $\delta^{18}O_{G.b.}$ and the shorter alkenone and pollen records from the same hole, when

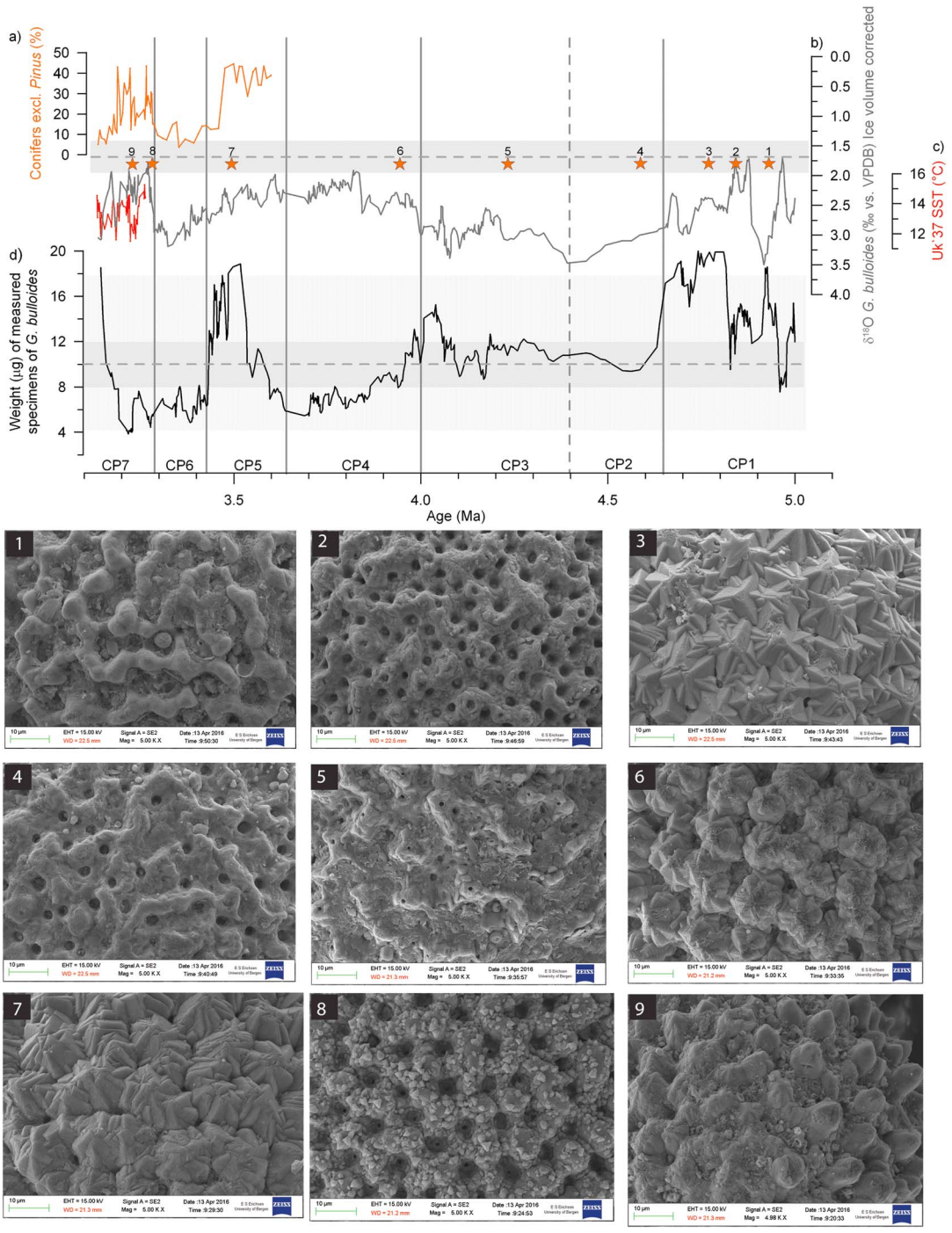

Figure 5. (a) Relative abundance of conifer pollen, excluding pines, in Hole 642B [*Panitz et al.*, 2016]. (b) Ice volume-corrected $\delta^{18}O_{G.b.}$ (five-point smoothed) with Holocene mean ($\pm 1\sigma$) indicated (see Figure 4 caption for details). The orange stars indicate from where the SEM pictures are taken. The number of each orange star refers to the numbers given on the SEM pictures. (c) Uk'37 SSTs from Hole 642B [*Bachem et al.*, 2016]. (d) Weight (µg) of measured specimens of *G. bulloides* (five-point smoothed). Horizontal dashed line and bars indicate Holocene mean and ranges (see Figure 4 caption and Table 2 for details) [*Dei Tos*, 2011]. Lower panel: SEM pictures from different extremes in the $\delta^{18}O_{G.b.}$ record, at 4.929, 4.837, 4.768, 4.585, 4.231, 3.940, 3.493, 3.268, and 3.231 Ma. Vertical grey lines indicate the timing of the transitions between the climate phases.

overlap occurs (Figure 5) [*Bachem et al*., 2016; *Panitz et al*., 2016]. These similarities indicate that the pattern of variability, if not the absolute values and amplitude of change in $\delta^{18}O_{G.b.}$, may still contain some climate information. Based on the combined SEM pictures and shell weight record (Figure 5), a first-order evaluation of the secondary effects is given for each CP.

CP1: SEM pictures 1–3 document variable overgrowth. The most severe overgrowths correspond with the highest shell weights. Pristine $\delta^{18}O_{G.b.}$ values are expected to be lower than those recorded, especially for the younger part of CP1, before entering CP2.
CP2: SEM picture 4 is less influenced by overgrowth than picture 3. Shell weights are similar to Holocene shell weights and lower than in CP1. The effect of diagenetic calcite on $\delta^{18}O_{G.b.}$ may be smaller during CP2 than during CP1, meaning that the pristine difference in $\delta^{18}O_{G.b.}$ between CP1 and CP2 may have been larger than indicated in Figure 5.
CP3: The degree of overgrowth indicated by SEM picture 5 is similar to picture 4 (CP2). The shell weights increase slightly compared to CP2. The $\delta^{18}O_{G.b.}$ values of CP3 may have been slightly more influenced by diagenetic calcite than during CP2, so that the lower $\delta^{18}O_{G.b.}$ values in CP3 compared to CP2 probably reflect a real difference.
CP4: More severe overgrowth is indicated by SEM picture 6 compared to 5 (CP3). The shell weights are comparable to CP3, even though shell weights, in general, were lower during CP4. The effect of diagenetic calcite was probably at least as strong as during CP3, and hence, the original difference between CP3 and CP4 was probably not smaller than indicated by the $\delta^{18}O_{G.b.}$ record.
CP5: Severe overgrowth (SEM picture 7) and high shell weights suggest that the original $\delta^{18}O_{G.b.}$ values were lower than measured. The relative $\delta^{18}O_{G.b.}$ difference between CP 4 and CP5 is not clear; hence, no interpretation can be made related to any change between the CPs. Due to the large change in shell weight within CP5, it is likely that the increasing trend in $\delta^{18}O_{G.b.}$ is caused by secondary effects rather than representing a pristine signal.
CP6: Less severe overgrowth is observed in SEM picture 8 compared to 7 (CP5), and lower shell weights are recorded. Hence, the effect of secondary processes was likely smaller during the CP6 than CP5, so that the pristine difference in $\delta^{18}O_{G.b.}$ between CP5 and CP6 was not smaller than measured.
CP7: The shell weights are comparable between CP6 and CP7. However, somewhat more overgrowth is indicated for CP7, based on SEM picture 9 versus 8. It is therefore likely that the original difference between CP6 and CP7 $\delta^{18}O_{G.b.}$ was at least as large as recorded.

The need for further investigations to verify these interpretations is stressed: no references to absolute $\delta^{18}O_{G.b.}$ values or amplitude changes should be made using the data from Hole 642B, and any paleoclimate interpretations must be treated with uttermost caution.

5.1.3. Would Diagenetic Calcite Also Influence the $\delta^{13}C_{G.b.}$, $\delta^{18}O_{C.t.}$ and $\delta^{13}C_{C.t.}$?

Since diagenetic calcite impacts planktic $\delta^{18}O$, one might expect a comparable effect on the $\delta^{13}C_{G.b.}$. To our knowledge no Pliocene studies have examined the potential effect of diagenetic calcite on planktic $\delta^{13}C$, but for a Miocene study the diagenetic impact was shown to be within the range of natural surface water variability between the investigated sites [*Edgar et al*., 2015]. For every carbon atom in $CaCO_3$ there are three oxygen atoms, so any overgrowth should in theory affect carbon isotopes less than oxygen isotopes. Furthermore, if the carbon isotopes were influenced by diagenetic calcite in the same way as the oxygen isotopes, by adding calcium carbonate with the same characteristics as the shallow pore water, a reduced $\Delta\delta^{13}C_{G.b.\text{-}C.t.}$ relative to the Holocene would be expected by adding $\delta^{13}C$-depleted $CaCO_3$ to the planktic foraminifera. The opposite is the case for the Pliocene $\delta^{13}C$ records, where a stronger contrast between the planktic and benthic $\delta^{13}C$ is observed during the Pliocene compared to the Holocene (Figure 4). Therefore, the $\delta^{13}C_{G.b.}$ values are likely similar to the original values derived from the surface waters, despite the impact of diagenetic calcite.

It is also likely that the benthic foraminifera were influenced by diagenetic calcite. However, the effect of diagenetic calcite on benthic $\delta^{18}O$ and $\delta^{13}C$ has been reported to be negligible, even when the foraminifera show some degree of textural changes due to recrystallization [*Edgar et al*., 2013; *Voigt et al*., 2016]. We therefore consider the $\delta^{18}O_{C.t.}$ and $\delta^{13}C_{C.t.}$ data sets to record trustworthy absolute values. However, given our evidence presented here for diagenetic effects, we emphasize that these records should also be considered with caution.

5.1.4. Differences Between Pliocene and Holocene $CaCO_3$ Preservation

The strong influence of diagenetic calcite on the planktic foraminifera from Hole 642B may be related to differences in carbonate preservation between the late Pleistocene and the Pliocene. At deeper depths in the Nordic Seas (ODP Site 907, 1800 m) the Pliocene sediment is barren of foraminifera [*Fronval and Jansen*, 1996], while the seafloor of the Nordic Seas lies entirely above the calcium carbonate compensation depth (CCD) at present and well-preserved foraminifera are found [*Hebbeln et al*., 1998; *Henrich*, 1986], even though some dissolution may occur underneath the colder water masses of the Greenland Sea [*Bauch et al*., 2001]. Due to the contrast between the Pliocene and the present carbonate preservation in the Nordic Seas, it is reasonable to assume that the CCD was located deeper than Hole 642B (1300 m) during the Pliocene, but at a shallower depth than at present, since corrosive bottom water caused dissolution of carbonate at deeper depths in the Nordic Seas [*Fronval and Jansen*, 1996]. Episodes of foraminifer barren intervals within the Pliocene, e.g., prior to 5.1 Ma and in part during CP2, suggest that Hole 642B may be located at a water depth close to the limit of where it is possible to get Pliocene foraminiferal-based reconstructions from the Nordic Seas.

5.1.5. Implications for Other Studies

The potential implications of our results for other studies should be stressed; we have shown that a severe influence of diagenetic calcite may occur at high-latitude sites and that the degree of diagenetic overgrowth changes with time, even over rather short timescales. The effect of diagenetic calcite on planktic $\delta^{18}O$ has previously been considered to be smaller at high-latitude sites with hemipelagic sediment than at tropical sites or sites from carbonate oozes [*Pearson and Burgess*, 2008; *Pearson et al*., 2001], even though *Williams et al*. [2005] found no clear trend between latitude or sediment type in a transect of cores through the Atlantic Ocean. Most studies investigating the effects of diagenetic calcite have focused on older sediment, e.g., of Eocene age [*Pearson et al*., 2001; *Sexton et al*., 2006]. We show here that careful consideration is also required of Pliocene sediments, when considering using isotopic records to reconstruct water mass properties.

5.2. $\delta^{13}C$ Proxy Interpretation

The $\delta^{13}C$ records are used to indicate changes in past ocean-atmosphere gas exchange, ocean ventilation, primary productivity, and decay of organic matter. Strong gas exchange between the ocean and the atmosphere is expressed through enriched $\delta^{13}C_{G.b.}$, as more ^{12}C is transferred to the atmosphere, while reduced ocean-atmosphere gas exchange is expressed by more depleted $\delta^{13}C_{G.b.}$, due to temperature-dependent equilibration between the ocean and the atmospheric pCO_2 [*Ravelo and Hillaire-Marcel*, 2007].

The Nordic Seas are presently one of the key deepwater formation sites and hence a well-ventilated ocean basin. If the ventilation of the Nordic Seas bottom waters were to decrease and more stagnant water would occupy the deeper parts of the basin, respiration will release CO_2 and consequently ^{12}C to the bottom water. Hence, reduced ventilation of the bottom water will be expressed by more depleted $\delta^{13}C_{C.t.}$. $\Delta\delta^{13}C_{G.b.\text{-}C.t.}$ gives an indication of the full water column at the site, with lower values indicating an improved subsurface to bottom water ventilation. More ^{12}C than ^{13}C is used during photosynthesis [*Ravelo and Hillaire-Marcel*, 2007], causing increased $\delta^{13}C$ in the water mass where the planktic foraminifera calcify, and hence, high primary productivity in the upper water column will cause enriched $\delta^{13}C_{G.b.}$. Respiration of organic matter will release ^{12}C to the bottom water masses as noted above. Strong decay of organic matter may therefore deplete the $\delta^{13}C_{C.t.}$, and hence, the $\Delta\delta^{13}C_{G.b.\text{-}C.t.}$ may also be influenced by biological processes.

Cassidulina teretis is a shallow infaunal benthic foraminifer species. The absolute values are thus not directly comparable with epifaunal *Cibicidoides wuellerstorfi* records from the North Atlantic [*Hodell and Venz-Curtis*, 2006]. Therefore, we only use the $\delta^{13}C_{C.t.}$ record at Hole 642B to investigate local changes in ocean ventilation and respiration of organic matter and to consider how these were different between the Pliocene and the Holocene.

5.3. Overarching Differences Between Pliocene and Holocene Climatic and Oceanographic Conditions in the Eastern Nordic Seas

Based on the generalized characteristics of the Hole 642B stable isotope records, it can be concluded that overall, the bottom waters of the Pliocene Nordic Seas were more dense (colder and/or saltier; see section 3 for more information on the link between $\delta^{18}O$ and density) relative to the Holocene mean and that

intensified ocean-atmosphere gas exchange took place in the upper water column (Figure 4). At the same time, the low $\delta^{13}C_{C.t.}$ combined with the lack of carbonate at deeper depths [*Jansen et al*., 2000] implies weaker deep convection in the Pliocene relative to the Holocene (Figure 4). These overarching differences between the Pliocene and the Holocene can be linked to boundary conditions of importance for the Nordic Seas oceanography that were consistently different between the two periods. Specifically, we discuss the higher atmospheric CO_2 concentrations, a lower Greenland Scotland Ridge (GSR), and a subaerial Barents Sea.

The Pliocene atmospheric CO_2 concentrations were higher than the preindustrial, and a long-term decreasing trend is indicated in several studies [*Badger et al*., 2013; *Bartoli et al*., 2011; *Martínez-Botí et al*., 2015; *Pagani et al*., 2010; *Pearson and Palmer*, 2000; *Seki et al*., 2010] (Figure 6). Through its impact on radiative forcing of global climate, a modulating effect of CO_2 changes on long-term climate changes and an influence on the Pliocene background climate state is expected. The generally high Pliocene $\delta^{13}C_{G.b.}$ and interpreted strong ocean-atmosphere gas exchange in the Nordic Seas are consistent with overall high atmospheric CO_2 concentrations and associated warmer SSTs. The low temporal resolution and large range in the reconstructed CO_2 values makes it difficult to directly compare the new data from Hole 642B, but the low-frequency climate variability recorded in the Nordic Seas is not reflected in the measured CO_2 data as presented. There are some similarities in the timing of the Nordic Seas climate transitions with shifts in a simulated CO_2 record [*Stap et al*., 2016]; e.g., the warming in the Nordic Seas into CP7 corresponds with a CO_2 increase (Figure 6). However, this simulation of atmospheric CO_2 relies on assumptions about the relationship between ice volume, sea level, and CO_2, using an inverse routine to interactively calculate CO_2 concentrations from benthic $\delta^{18}O$. To better understand the potential role played by atmospheric CO_2 in the long-term variability expressed in the Nordic Seas, data will require the production of high-resolution CO_2 reconstructions.

The Greenland Scotland Ridge (GSR) was about 250 m deeper than today throughout the Pliocene [*Poore et al*., 2006]. Using the HadCM3 climate model, *Robinson et al*. [2011] showed that an 800 m deeper GSR sill depth strengthened and deepened the Atlantic Meridional Overturning Circulation (AMOC) and increased temperatures throughout the Nordic Seas water column. The generally dense bottom water documented by the Hole 642B record is not consistent with warming of the entire water column (Figures 4 and 6). The lack of carbonate in the deep Nordic Seas, interpreted as an effect of reduced ventilation [*Jansen et al*., 2000], is also inconsistent with a strengthened and deepened AMOC. Using a more realistic GSR sill depth (330 m deeper than today), *Hill* [2015] found the same warming pattern as *Robinson et al*. [2011], but with a reduced amplitude. A 250 m deeper Pliocene GSR sill depth likely influenced the Nordic Seas oceanography in a constant way by increasing the surface temperatures. Based on new alkenone SSTs from the Norwegian Sea [*Bachem et al*., 2016] (Figure 5), the temperature estimate of *Hill* [2015] seems to be the most realistic for the late Pliocene. The exact effect in the deeper parts of the water column still needs to be better constrained, in light of the inconsistencies between our stable isotope records and the modeling results from *Hill* [2015] and *Robinson et al*. [2011].

The Barents Sea was subaerially exposed throughout the Pliocene [*Butt et al*., 2002], and the Canadian Arctic Archipelago was closed [*Matthiessen et al*., 2009]. Hence, the Fram Strait and the Bering Strait were the only open gateways to the Arctic Ocean. Presently, the Barents Sea is one of the main pathways of Atlantic water transport toward the Arctic and an area of substantial heat loss to the atmosphere [*Smedsrud et al*., 2013]. Through brine water formation, the Barents Sea contributes to the formation of the densest fraction of the North Atlantic Deep Water. If the Barents Sea is land, as during the Pliocene, the bifurcation of the NwAC is hampered, in turn increasing heat transport to the Arctic Ocean through the Fram Strait [*Butt et al*., 2002; *Hill*, 2015]. Increased heat transport to the Arctic Ocean and decreased influence of brine water as a factor for deep water formation may have had wider climatic and oceanographic implications, e.g., through reduced deep water ventilation. Reduced Pliocene deep water ventilation in the Nordic Seas is supported by our data and previous studies, suggesting a vigorous circulation in the upper water column, but no strong deep convection (Figures 4 and 6) [*Jansen et al*., 2000]. Furthermore, our data from Hole 642B support the model study by *Hill* [2015], who identified reduced AMOC strength even though the heat transport to the Arctic Ocean increased as a response to a subaerial Barents Sea.

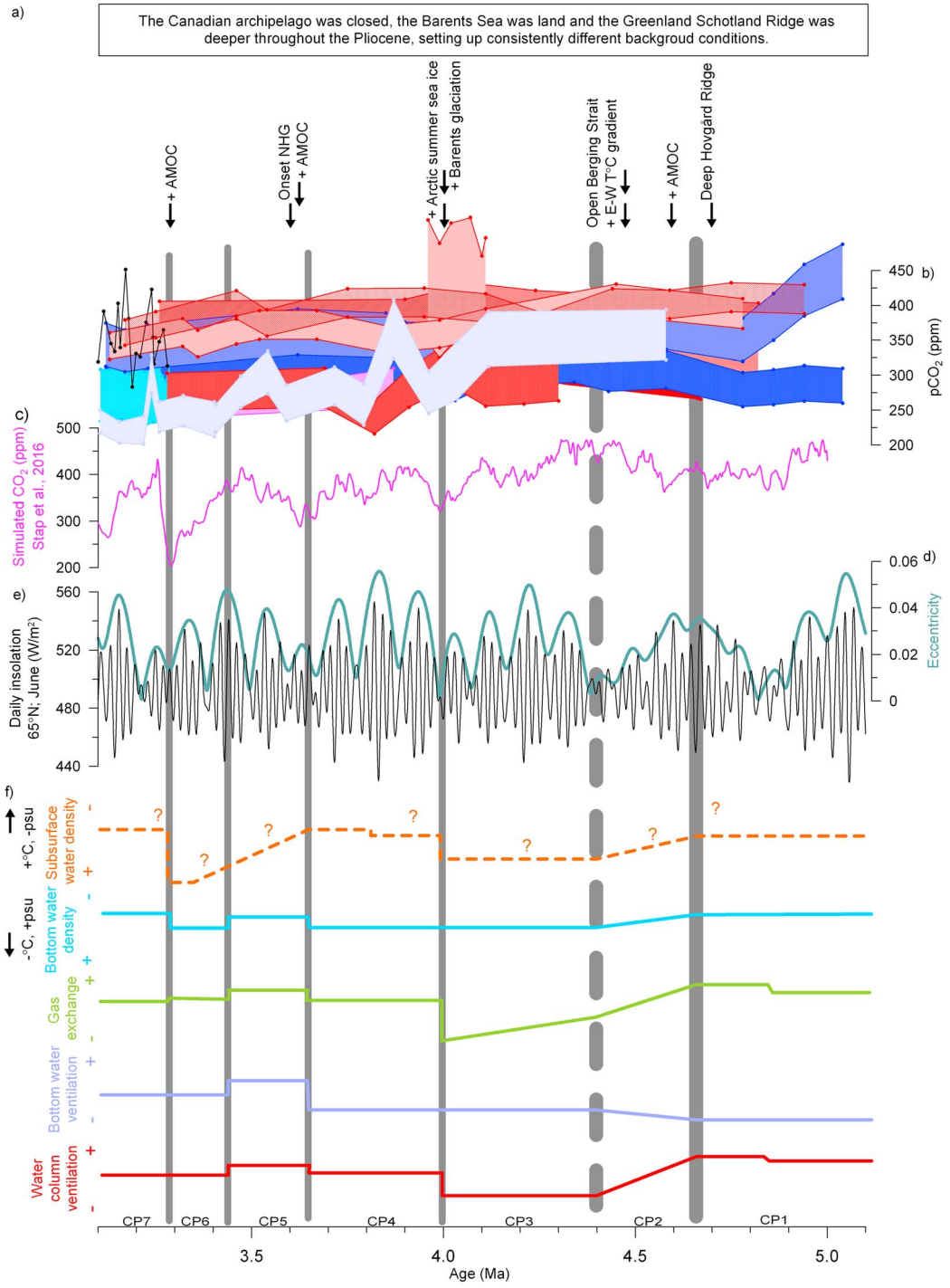

Figure 6. Summarizing discussed factors of potential influence on the Pliocene eastern Nordic Seas oceanography. (a) Timing of paleogeographic changes and related paleoceanographic changes of potential importance for explaining the climate transitions documented in Hole 642B. (b) Reconstructed pCO_2 data as found in the literature [*Badger et al.*, 2013; *Bartoli et al.*, 2011; *Martínez-Botí et al.*, 2015; *Pagani et al.*, 2010; *Pearson and Palmer*, 2000; *Seki et al.*, 2010]. The different colors represent the different references (powder blue [*Bartoli et al.*, 2011], neon purple [*Pearson and Palmer*, 2000], sky blue [*Badger et al.*, 2013], blue [*Seki et al.*, 2010], red [*Pagani et al.*, 2010], and black [*Martínez-Botí et al.*, 2015]). (c) Simulated pCO_2 [*Stap et al.*, 2016], (d) eccentricity [*Laskar et al.*, 2004], and (e) June insolation at 65°N. (f) A schematic overview of water column changes as seen in the Hole 642B records is shown in the lower part of the figure. Subsurface water density changes are indicated based on $\delta^{18}O_{G.b.}$ (dashed line and question marks are included to emphasize the large uncertainty related to interpreting this record), bottom water density from $\delta^{18}O_{C.t.}$. Gas exchange is defined by $\delta^{13}C_{G.b.}$. Bottom water ventilation is based on the interpretations of $\delta^{13}C_{C.t.}$. Water column ventilation is derived from $\Delta\delta^{13}C_{G.b.\text{-}C.t.}$. Vertical grey lines indicate the timing of the transitions between the climate phases. The stippled vertical line indicates the larger uncertainty related to the transition between CP1 and CP2. The thickness of the grey lines reflects the age uncertainties for different Pliocene intervals as indicated by *Lisiecki and Raymo* [2005], 30 ky between 5 and 4 Ma and 15 ky between 4 and 3 Ma.

5.4. Pliocene Climate Phases and Connections to Paleogeographical and Paleoceanographic Changes and the Onset of Northern Hemisphere Glaciation

5.4.1. Climate Phase 1 (CP1, 5.05–4.65 Ma) and the Transition Toward CP2

During CP1, $\delta^{18}O_{G.b.}$ and $\delta^{18}O_{C.t.}$ indicate variable surface and bottom water densities. The $\delta^{18}O_{G.b.}$ record is strongly influenced by secondary processes (section 5.1) and should only be considered with high level of caution. The largest IRD peak, circa 4.8–4.9 Ma (Figure 4), corresponds to a globally recognized glaciation event [*De Schepper et al*., 2014], supporting temperature as a driver behind the density change, since fresh meltwater associated with the increase in IRD would have operated in the reverse sense, by decreasing the density signal. The highest $\delta^{13}C_{G.b.}$ and lowest $\delta^{13}C_{C.t.}$ correspond with increased primary productivity at Hole 642B as indicated from a low-resolution record of dinoflagellate cyst and acritarch accumulation rates (based on *De Schepper et al*. [2015]) (Figure 4), indicating an influence of productivity and decay of organic matter on the $\delta^{13}C_{G.b.}$ and $\delta^{13}C_{C.t.}$, respectively. However, this relationship between carbon isotopes and accumulation rates is not constant through CP1, implying that increased ocean-atmosphere gas exchange and reduced bottom water ventilation were likely more important.

The transition into CP2 (circa 4.65 Ma) roughly corresponds to subsidence of the Hovgård Ridge and increased AMOC. The Hovgård Ridge in the Fram Strait may have been elevated until the late Miocene, partly restricting the flow through the Fram Strait as it gradually subsided until 4.7 Ma [*Knies et al*., 2014b]. A restricted (nonrestricted) exchange through the Fram Strait may have caused a stronger (weaker) RAC prior to (after) 4.7 Ma. The oceanographic changes linked to reduced exchange through the Fram Strait, in combination with the effects of a subaerial Barents Sea, could therefore have been important for creating the less dense and less well-ventilated bottom water before 4.65 Ma (Figure 4). However, it has also been argued that the Fram Strait was already wide and deep enough by 17.5–13.7 Ma to establish a good ventilation of the Arctic Ocean [*Jakobsson et al*., 2007]. In that case, no effect would be expected in the Nordic Seas.

The Caribbean and North Atlantic became gradually warmer and saltier from circa 4.6 Ma, enhancing the AMOC [*Haug and Tiedemann*, 1998; *Sarnthein et al*., 2009] (Figure 6), although the exact mechanism behind the enhanced AMOC is still discussed [*Haug and Tiedemann*, 1998; *Lunt et al*., 2008; *Mestas-Nunez and Molnar*, 2014; *Sarnthein et al*., 2009]. Regardless of the underlying driver, an intensified AMOC from circa 4.6 Ma would have brought warmer and saltier water to the North Atlantic, leading to a more evaporative high-latitude ocean and consequently increased salinities. Despite the influence of secondary processes on $\delta^{18}O_{G.b.}$, there is a trend toward increased surface densities at Hole 642B after 4.65 Ma, which may be influenced by such a salinity increase. In that case most of the heat must have been released to the atmosphere before reaching the Nordic Seas, since the warm water would have led to a reduction in density (Figures 4 and 6).

5.4.2. Climate Phase 2 (CP2, 4.65–4.4 Ma) and the Transition Toward CP3

CP2 was distinct from CP1 and CP3, but its oceanographic conditions are less clear. The surface water density possibly increased from CP1, while the bottom water conditions are indicated to have been similar to the Holocene mean. There was a gradual reduction in primary production through CP2, seen both in $\delta^{13}C_{G.b.}$ and the accumulation rate of dinoflagellate cysts and acritarchs (based on *De Schepper et al*. [2015]), contributing to the increase in $\delta^{13}C_{C.t.}$ (Figure 4).

The transition into CP3, at circa 4.4 Ma, is less well defined than the other transitions, due to the scarce information available for CP2, but it occurred shortly after or together with the establishment of a strong E-W SST gradient in the Nordic Seas [*De Schepper et al*., 2015] (Figure 6). Contemporaneous with the first occurrence of Pacific mollusks in the Nordic Seas from circa 4.5 Ma, the EGC likely cooled and freshened, linked to inflow of fresh Pacific water via the Bering Strait [*De Schepper et al*., 2015]. Since the Canadian Archipelago was closed, more fresh Pacific-sourced water entered the EGC than today. As a consequence, an E-W temperature gradient developed in the Nordic Seas, with a well-defined NwAC and EGC [*De Schepper et al*., 2015]. It is also suggested that an erosional unconformity at the Erik Drift created at circa 4.5 Ma resulted from stronger deep currents linked to an intensified Denmark Strait Overflow [*Bohrmann et al*., 1990; *Müller-Michaelis et al*., 2013]. Establishing an intensified Denmark Strait Overflow after 4.5 Ma is in agreement with the eastern Nordic Seas ocean ventilation being comparable to the Holocene after circa 4.4 Ma, as is indicated by Hole 642B $\Delta\delta^{13}C_{G.b.-C.t.}$ (Figures 4 and 6).

5.4.3. Climate Phase 3 (CP3, 4.4–4.0 Ma) and the Transition Toward CP4

During CP3, the bottom water was more dense than during CP2. The Pliocene minimum in primary production and/or ventilation of the upper water column was at 4.1 Ma. Low primary productivity, as indicated by $\delta^{13}C_{G.b.}$, is supported by decreased accumulation rates of dinoflagellate cysts and acritarchs in Hole 642B (based on *De Schepper et al*. [2015]), relative to earlier in the Pliocene (Figure 5). The higher $\delta^{13}C_{C.t.}$ indicate better bottom water ventilation than earlier in the Pliocene and slightly lower than the Holocene mean. Comparable $\Delta\delta^{13}C_{G.b.\text{-}C.t.}$ to the Holocene indicates that the eastern Nordic Seas was better ventilated, and hence, a deeper overturning circulation likely took place, through CP3 than at any other time during the Pliocene (Figures 4 and 6).

The transition between CP3 and CP4, at circa 4 Ma, corresponds to a distinct change in sediment provenance at the Yermak Plateau following a gradual long-term climatic cooling and initial glacial buildup [*Knies et al*., 2014b]. The occurrence of glaciers on Svalbard and seasonal sea ice at the Yermak Plateau from 4 Ma [*Knies et al*., 2014a] both suggest at least seasonal Arctic cooling. The observed response at Hole 642B at 4 Ma (Figures 5 and 6) is consistent with a warmer NwAC which can be linked to sea ice expansion. An increased Arctic sea ice extent at 4 Ma might have increased the transport of sea ice, and hence the freshwater flux, to the Nordic Seas, through the Fram Strait and the East Greenland Current. Increased freshwater flux to the western Nordic Seas and the North Atlantic from the Arctic may in turn cause enhanced transport of warm and salty Atlantic water to the eastern Nordic Seas [*Otterå and Drange*, 2004]. Hence, more Arctic Sea ice may have been important for the warming at Hole 642B around 4 Ma.

5.4.4. Climate Phase 4 (CP4, 4.0–3.65 Ma) and the Transition Toward CP5

The $\delta^{18}O_{G.b.}$ and $\delta^{18}O_{C.t.}$ records indicate that surface water density was reduced during CP4, acknowledging the strong diagenetic alteration of $\delta^{18}O_{G.b.}$ (section 5.1), while the bottom water remained as dense as during CP3 (Figure 5). This time interval corresponds to when the warmest Pliocene SSTs are recorded in the North Atlantic [*Federov et al*., 2013; *Lawrence et al*., 2009]. Hence, it may be reasonable to assume that the possible lower surface water densities were linked to the high temperatures of Atlantic water entering the Nordic Seas. The carbon isotope records show that gas exchange/ventilation of the upper water column increased rapidly when entering CP4 and stayed strong, while the bottom water ventilation stayed reduced. The increased ocean-atmosphere gas exchange would also be consistent with increased ocean temperatures.

5.4.5. Climate Phase 5 (CP5, 3.65–3.42 Ma) and the Transition Toward CP6

The $\delta^{18}O_{C.t.}$ record from Hole 642B shows that the bottom water density remained close to Holocene mean values during CP5. A surface density increase, potentially linked to decreasing temperatures, is indicated, in line with the gradual intensification of Northern Hemisphere glaciation (NHG) from 3.6 Ma (Figure 6) [*Mudelsee and Raymo*, 2005]. This interpretation has, however, low confidence, due to the uncertain effect of diagenetic calcite through CP5 and requires further testing with alternative surface water proxies. The $\delta^{13}C_{G.b.}$ values were higher than any recorded in the Holocene yet in contrast to CP1 the high $\delta^{13}C_{G.b.}$ values are not associated with high accumulation rates of dinoflagellate cysts and acritarchs (Figure 4). Hence, strong ocean-atmosphere gas exchange may have taken place. Changes in Hole 642B $\delta^{13}C_{C.t.}$ indicate strong overturning circulation due to better ventilation of the bottom water during CP5, in line with arguments for an intensified AMOC [*Haug and Tiedemann*, 1998; *Lunt et al*., 2008; *Sarnthein et al*., 2009].

The transition between CP5 and CP6, at circa 3.42 Ma, does not correspond with any known gateway changes (Figure 6), but it is also reflected in a shift toward colder vegetation in Northern Norway [*Panitz et al*., 2016] (Figure 5) and a cooling step seen in the temperature record from Lake El'gygytgyn [*Brigham-Grette et al*., 2013]. These similarities hint at hemispheric-wide high-latitude cooling at the transition between CP5 and CP6, although the cause is uncertain.

5.4.6. Climate Phase 6 (CP6, 3.42–3.285 Ma) and the Transition Toward CP7

While $\delta^{18}O_{C.t.}$ indicate that the bottom water remained dense throughout CP6, the surface density is indicated to have increased until circa 3.35 Ma. We have noted the large uncertainty linked to this interpretation of $\delta^{18}O_{G.b.}$ given the evidence for diagenetic alteration of the calcite (section 5.1), but the pattern would be consistent with a cooling initiated following the onset of NHG from 3.6 Ma [*Mudelsee and Raymo*, 2005] toward the MIS M2 glaciation at circa 3.3 Ma. The $\delta^{13}C_{C.t.}$ shows stable conditions throughout CP6, comparable to the Holocene mean. The water column is indicated to have been well ventilated but slightly less so than during CP5.

The transition between CP6 and CP7, at circa 3.285 Ma, corresponds with the deglaciation of the MIS M2 glaciation. It is suggested that the MIS M2 deglaciation occurred as a response to expansion and warming of the Caribbean warm pool essential for a reestablishment of strong AMOC and northward heat transport through the North Atlantic Current [*De Schepper et al*., 2013]. Buildup of surplus heat in the tropics is also suggested to be important for late Quaternary deglaciations [*Rühlemann et al*., 1999]. The suggested decrease in density at Hole 642B associated with this transition is likely associated with warmer temperatures in the eastern Nordic Seas (Figure 4). Warmer Nordic Seas are also in line with establishment of a warmer vegetation in Northern Norway [*Panitz et al*., 2016] (Figure 5) and from Lake El'gygytgyn [*Brigham-Grette et al*., 2013], again, hinting at a hemispheric-wide high-latitude response.

5.4.7. Climate Phase 7 (CP7, 3.285–3.14 Ma)

During CP7, variable surface water conditions are indicated at Hole 642B. Despite the impact of diagenetic calcite on $\delta^{18}O_{G.b.}$, both surface and bottom water densities were likely lower than during CP6 (Figures 4 and 5). A slightly reduced ocean-atmosphere gas exchange is indicated by the $\delta^{13}C_{G.b.}$, relative to the preceding CPs, but it was still at the high end of Holocene values. With the exception of an event at 3.23 Ma when both $\delta^{13}C_{G.b.}$ and $\delta^{18}O_{C.t.}$ experienced a sharp decrease, the bottom water ventilation was comparable to the Holocene and, hence, well ventilated. Of all the Pliocene CPs, bottom water conditions were most similar to Holocene conditions during CP7.

5.5. How Do the Pliocene Climate Phases and the Transitions Link to Insolation Forcing?

As outlined in section 5.4, the new Pliocene climate records from the eastern Nordic Seas document low-frequency changes in the characteristics of the water column. Seven climate phases lasting between 150,000 and 400,000 years, with distinct characteristics, are identified. Transitions between these phases cannot be explained solely by changes to atmospheric CO_2 concentrations and/or gateway changes. The onset of four of these climate phases, CP3, CP4, CP5, and CP7, occurred close to an amplitude minimum of Northern Hemisphere summer insolation and a minimum in eccentricity (Figure 6). The pre-Pleistocene existence of low-frequency, large-amplitude changes in stable isotope records, linked to eccentricity, is known from tropical areas [*Clemens and Tiedemann*, 1997; *Zachos et al*., 1997]. It has been suggested that changes in continental geography and the land versus sea distribution may have a filtering effect that influences the amplification of the power in the eccentricity band [*Short et al*., 1991]. However, it is not clear how the effects of eccentricity on the tropics should be exported to high northern latitudes [*Zachos et al*., 2008]. In contrast, the onset of CP2 and CP6 occurs at the maximum amplitude of the insolation changes, corresponding to maximum eccentricity (Figure 6). These transitions may be influenced by intensified seasonality related to the insolation forcing, in agreement with the potential decreases in temperatures indicated by the $\delta^{18}O_{G.b.}$ increases. Further work is required to better understand how these shorter windows of specific insolation forcing might be translated into the climate phases, which have longer duration and so may indicate some form of threshold response to shorter-timescale changes.

5.6. Summarizing: Paleogeography and/or Insolation Forcing?

The isotope records from Hole 642B detail a series of climate phases, and transitions between them, which are not comparable in their responses, even though the onset of several CPs occurs under comparable insolation forcing. Therefore, it is likely that the observed climate transitions result from a combination of low-frequency insolation forcing and even slower, long-term tectonic changes. We reiterate here that due to variable impacts of diagenesis on the planktic foraminifer calcite, both the absolute values and amplitudes of change across these transitions may have been compromised, especially in $\delta^{18}O_{G.b.}$. Despite this, most of our defined climate transitions and inherent changes to the Nordic Seas oceanography can be linked to one or several known paleogeographic/paleoceanographic changes, changes in Arctic sea ice cover, and/or the onset of Northern Hemisphere glaciation (Figure 6). As the perennial Arctic Ocean sea ice cover expanded to cover larger areas after 4 Ma, and the Northern Hemisphere ice sheets grew bigger following 3.6 Ma, feedback mechanisms related to albedo changes might also have been of importance. It is also important to consider that all of these interactions occurred on top of background conditions that were different to those of the present interglacial. There remains a need for further investigations of (1) the mechanistic linkages between the changing boundary conditions and the Pliocene Nordic Seas oceanography and (2) how the combination of gradual long-term changes of the external and internal forcing may lead to threshold behavior.

6. Conclusions

The first suborbitally resolved planktic and benthic oxygen and carbon isotope records of Pliocene age from the Nordic Seas are presented. The records are discussed in relation to preservation of Pliocene foraminifera in the Nordic Seas, overarching differences between Pliocene and Holocene climatic and oceanographic conditions in the eastern Nordic Seas, low-frequency climate variability, and how these are associated with changes in external and internal forcing. Specifically, we show the following:

1. An influence of secondary calcite is documented on *G. bulloides*, and we emphasize the need to be cautious regarding the interpretations of the stable isotope records we present. We show that the impact is likely to be strongest on $\delta^{18}O_{G.b.}$ but could also have influenced the other stable isotope records, even though they are likely less sensitive to the diagenetic effects. Further studies and multiproxy analyses are needed to evaluate the Pliocene Nordic Seas oceanography with improved confidence.
2. The role played by atmospheric CO_2 in the long-term variability expressed in Hole 642B cannot be understood with the presently available CO_2 data.
3. The carbon isotope records from Hole 642B support previous studies suggesting a vigorous circulation in the upper water column, but no strong deep convection in the Nordic Seas during the Pliocene.
4. The weaker ventilation of the deep Nordic Seas may in part be linked to strong poleward heat transport and reduced brine formation due to a subaerial Barents Sea.
5. Seven phases with different climatic and oceanographic conditions are identified between 5.05 and 3.14 Ma, each lasting between 400,000 and 150,000 years.
6. Four of the transitions between the defined climate phases occurred close to an eccentricity minimum and a minimum in amplitude of change for Northern Hemisphere summer insolation, while two occurred around an eccentricity maximum and a maximum in amplitude in insolation change.
7. In addition to insolation, changes in paleogeography and related paleoceanographic and paleoclimatic changes were players behind the evolving Pliocene low-frequency variability climate in the eastern Nordic Seas (e.g., subsidence of the Hovgård Ridge until circa 4.7 Ma; strengthened AMOC at circa 4.6, circa 3.6, and circa 3.3 Ma; and opening of the Bering Strait and establishment of an E-W surface temperature gradient comparable to the present from circa 4.5 Ma, as well as the onset of Barents glaciation and expanded Arctic sea ice cover from circa 4 Ma and onset of NHG from circa 3.6 Ma).
8. The mechanistic linkages between changing boundary conditions and the Pliocene Nordic Seas oceanography, and how the combination of gradual long-term changes of the external and internal forcing, and feedbacks between them, may lead to threshold behavior will need further investigation.

Acknowledgments

Samples for this study were provided by ODP. We thank D. Bøe, R. Søraas, O. Hansen, D.I. Blindheim, L. Elvik, and L. Jensen for technical assistance. E.S. Erichsen, I. Polovodva Asteman, A. Breistøl, and K. Meland helped with the SEM pictures. The study was financed through the projects Earth System Modeling, NFR project 221712 (OCCP) and the Centre for Climate Dynamics at the Bjerknes Centre through the DYNAWARM project. S.D.S. acknowledges funding from NFR project 229819 (PEGSIE), and E.L.M. acknowledges funding through a Philip Leverhulme Prize. The data are available at https://doi.pangaea.de/10.1594/PANGAEA.863867. Comments from two anonymous reviewers and Bärbel Hönisch improved the manuscript significantly.

References

Bachem, P., B. Risebrobakken, and E. L. McClymont (2016), Sea surface temperature variability in the Norwegian Sea during the late Pliocene linked to subpolar gyre and radiative forcing, *Earth Planet. Sci. Lett.*, *446*, 113–122.

Badger, M. P. S., D. N. Schmidt, A. Mackensen, and R. D. Pancrost (2013), High-resolution alkenone paleobarometry indicates relatively stable pCO_2 during the Pliocene (3.3–2.8 Ma), *Philos. Trans. R. Soc. London, Ser. A*, *371*(2001), 20130094, doi:10.1098/rsta.2013.0094.

Bartoli, G., B. Hönisch, and R. E. Zeebe (2011), Atmospheric CO_2 decline during the Pliocene intensification of Northern Hemisphere glaciations, *Paleoceanography*, *26*, PA4213, doi:10.1029/2010PA002055.

Bauch, H., A. H. Erlenkauser, R. F. Spielhagen, U. Struck, J. Matthiessen, J. Thiede, and J. Heinemeier (2001), A multiproxy reconstruction of the evolution of deep and surface waters in the Nordic Seas over the last 30,000 years, *Quat. Sci. Rev.*, *20*(6), 659–678.

Berggren, W. A., D. V. Kent, and J. A. Couvering, (1985), Neogene geochronology and chronostratigraphy, in *The Chronology of the Geological Record*, edited by N. J. Snelling, *Mem. Geol. Soc. London*, 10, 141–195.

Bleil, U. (1989), Magnetostratigraphy of Neogene and Quaternary sediment series from the Norwegian Sea: Ocean Drilling Program, Leg 104, in *Proceedings of the Ocean Drilling Program, Scientific Results, 104*, edited by O. Eldholm et al., pp. 829–901, Ocean Drilling Program, College Station, Tex.

Blindheim, J., and S. Østerhus (2005), The Nordic Seas, main oceanographic features, in *The Nordic Seas: An Integrated Perspective*, edited by H. Drange et al., pp. 11–38, AGU, Washington, D. C.

Bohrmann, G., R. Henrich, and J. Thiede (1990), Miocene to Quaternary paleoceanography in the northern North Atlantic: Variability in carbonate and biogenic opal accumulation, in *Geological History of the Polar Oceans: Arctic Versus Antarctic*, *NATO ASI Series*, edited by U. Bleil and J. Thiede, pp. 647–676.

Bolton, C. T., P. A. Wilson, I. Bailey, O. Friedrich, C. J. Beer, J. Becker, S. Baranwal, and R. Schiebel (2010), Millennial-scale climate variability in the subpolar North Atlantic Ocean during the late Pliocene, *Paleoceanography*, *25*, PA4218, doi:10.1029/2010PA001951.

Brigham-Grette, J., et al. (2013), Pliocene warmth, polar amplification, and stepped Pleistocene cooling recorded in NE Arctic Russia, *Science*, *340*, 1421–1427, doi:10.1126/science.1233137.

Buchardt, B., and L. A. Símonarson (2003), Isotope palaeotemperatures from the Tjörnes beds in Iceland: Evidence of Pliocene cooling, *Paleogeogr. Paleoclimatol. Paleoecol.*, *189*, 71–95.

Butt, F. A., H. Drange, A. Elverhøi, O. H. Otterå, and A. Solheim (2002), Modelling Late Cenozoic isostatic elevation changes in the Barents Sea and their implications for oceanic and climatic regimes: Preliminary results, *Quat. Sci. Rev.*, *21*, 1643–1660.

Cande, S. C. and D. V. Kent (1995), Revised calibration of the geomagnetic polarity timescale for the Late Cretaceous and cenozoic, *J. Geophys. Res.*, *100*(B4), 6093–6095.

Clemens, S. C., and R. Tiedemann (1997), Eccentricity forcing of Pliocene-Early Pleistocene climate revealed in a marine oxygen-isotope record, *Nature*, *385*, 801–804.

Cronin, T. M. (1991), Late Neogene marine Ostracoda from Tjörnes, Iceland, *J. Paleontol.*, *65*(5), 767–794.

De Schepper, S., and M. J. Head (2008), Age calibration of dinoflagellate cyst and acritarch events in the Pliocene-Pleistocene of the eastern North Atlantic (DSDP Hole 610A), *Stratigraphy*, *5*(2), 137–161.

De Schepper, S., J. Groeneveld, B. D. A. Naafs, C. Van Renterghem, J. Hennissen, M. J. Head, S. Louwye, and K. Fabian (2013), Northern Hemisphere glaciation during the globally warm early late Pliocene, *PLoS One*, *8*(12), e81508, doi:10.81371/journal.pone.0081508.

De Schepper, S., P. L. Gibbard, U. Salzmann, and J. Ehlers (2014), A global synthesis of the marine and terrestrial evidence for glaciation during the Pliocene Epoch, *Earth Sci. Rev.*, *135*, 83–102.

De Schepper, S., M. Schreck, K. M. Beck, J. Matthiessen, K. Fahl, and G. Mangerud (2015), Early Pliocene onset of modern Nordic Seas circulation related to ocean gateway changes, *Nat. Comm.*, *6*, 8659, doi:10.1038/ncomms9659.

de Villiers, S. (2003), A 425 kyr record of foraminiferal shell weight variability in the western equatorial Pacific, *Paleoceanography*, *18*(4), 1080, doi:10.1029/2002PA000801.

Dei Tos, L. (2011), Holocene surface ocean conditions of the Norwegian Sea as recorded by *Globigerina bulloides* (Mg/Ca ratios and $\delta^{18}O$), Master thesis, Universitá degli studi di Padova, 50 pp.

Dokken, T. M., and E. Jansen (1999), Rapid changes in the mechanism of ocean convection during the last glacial period, *Nature*, *401*, 458–461.

Dowsett, H. J., et al. (2013), Sea surface temperature of the mid-Piacenzian ocean: A data-model comparison, *Sci. Rep.*, *3*, doi:10.1038/srep02013.

Dreger, D. (1999), *Decadal-to-Centennial-Scale Sediment Records of Ice Advance on the Barents Shelf and Meltwater Discharge Into the Northeastern Norwegian Sea Over the Last 40 Kyr*, pp. 71, Christian-Albrechts-Univ., Kiel.

Edgar, K. M., H. Pälike, and P. A. Woilson (2013), Testing the impact of diagenesis on the $\delta^{18}O$ and $\delta^{13}C$ of benthic foraminiferal calcite from a sediment burial depth transect in the equatorial Pacific, *Paleoceanography*, *28*, 468–480, doi:10.1029/palo.20045.

Edgar, K. M., E. Anagnostou, P. N. Pearson, and G. L. Foster (2015), Assessing the impact of diagenesis on $\delta^{11}B$, $\delta^{13}C$, $\delta^{18}O$, Sr/Ca and Ba/Ca values in planktic foraminiferal calcite, *Geochem. Cosmochem. Acta*, *166*, 189–209.

Ezard, T. H., K. M. Edgar, and P. M. Hull (2015), Environmental and biological controls on size-specific $\delta^{13}C$ and $\delta^{18}O$ in recent planktonic foraminifera, *Paleoceanography*, *30*, 151–173, doi:10.1002/2014PA002735.

Fairbanks, R. G. (1989), A 17,000-year glacio-eustatic sea level record: Influence of glacial melting rates on the Younger Dryas event and deep-ocean circulation, *Nature*, *342*, 637–642.

Federov, A. V., P. S. Dekens, M. McCarthy, A. C. Ravelo, P. B. de Menocal, M. Barreiro, R. C. Pacanowski, and S. G. Philander (2006), The Pliocene paradox (mechanisms for a permanent El Niño), *Science*, *312*, 1485–1489.

Federov, A. V., C. Brierley, K. T. Lawrence, Z. Liu, P. S. Dekens, and A. C. Ravelo (2013), Patterns and mechanisms of early Pliocene warmth, *Nature*, *496*, 43–52.

Fronval, T., and E. Jansen (1996), Late Neogene paleoclimates and paleoceanography in the Iceland-Norwegian Sea: Evidence from the Iceland and Vøring Plateaus, *Proc. Ocean Drill. Prog. Sci Results*, *151*, 455–468.

Furevik, T., and J. E. Ø. Nilsen (2005), Large-scale atmospheric circulation variability and its impacts on the Nordic Seas ocean climate—A review, in *The Nordic Seas: An Integrated Perspective*, *Geophys. Monogr. Ser.*, vol. 158, edited by H. Drange et al., pp. 105–136, AGU, Washington, D. C.

Haug, G. H., and R. Tiedemann (1998), Effect of the formation of the Isthmus of Panama on Atlantic Ocean thermohaline circulation, *Nature*, *393*, 673–676.

Haywood, A. M., A. Ridgwell, D. J. Lunt, D. J. Hill, M. J. Pound, H. J. Dowsett, A. M. Dolan, J. A. Francis, and M. Williams (2011), Are there pre-Quaternary geological analogues for a future greenhouse warming?, *Philos. Trans. R. Soc. London, Ser. A*, *369*, 933–956.

Hebbeln, D., R. Henrich, and K.-H. Baumann (1998), Paleoceanography of the last interglacial/glacial cycle in the polar North Atlantic, *Quat. Sci. Rev.*, *17*, 125–153.

Henrich, R. (1986), A calcite dissolution pulse in the Norwegian-Greenland Sea during the last deglaciation, *Geol. Rundsch.*, *75*(3), 805–827.

Hilgen, F. J., L. J. Lourens, and J. A. van Dam (2012), The Neogene period, in *The Geologic Time Scale 2012 2-Volume Set*, vol. 2, edited by F. M. Gradstein et al., pp. 923–978, Elsevier, Boston.

Hill, D. (2015), The non-analogue nature of Pliocene temperature gradients, *Earth Planet. Sci. Lett.*, *425*, 232–241.

Hodell, D. A., and K. A. Venz-Curtis (2006), Late Neogene history of deepwater ventilation in the Southern Ocean, *Geochem. Geophys. Geosyst.*, *7*, Q09007, doi:10.1029/02005GC001211.

Jakobsson, M., et al. (2007), The early Miocene onset of a ventilated circulation regime in the Arctic Ocean, *Nature*, *447*(7147), 986–990, doi:10.1038/Nature05924.

Jansen, E., U. Bleil, R. Henrich, L. Kringstad, and B. Slettemark (1988), Paleoenvironmental changes in the Norwegian Sea and the northeast Atlantic during the last 2.8 m.y.: Deep Sea Drilling Project/Ocean Drilling Program Sites 610, 642, 643 and 644, *Paleoceanography*, *3*, 563–581, doi:10.1029/PA003i005p00563.

Jansen, E., J. Sjøholm, U. Bleil, and J. A. Erichsen (1990), Neogene and Pleistocene glaciations in the northern hemisphere and late Miocene-Pliocene global ice volume fluctuations: Evidence from the Norwegian Sea, in *Geological History of the Polar Oceans: Arctic Versus Antarctic*, edited by U. Bleil and J. Thiede, pp. 677–705, Kluwer Acad., Netherlands.

Jansen, E., T. Fronval, F. Rack, and J. E. T. Channell (2000), Pliocene-Pleistocene ice rafting history and cyclicity in the Nordic Seas during the last 3.5 Myr, *Paleoceanography*, *15*, 709–721, doi:10.1029/1999PA000435.

Knies, J., P. Cabedo-Sanz, S. T. Belt, S. Baranwal, S. Fietz, and A. Rosell-Melé (2014a), The emergence of modern sea ice cover in the Arctic Ocean, *Nat. Comm.*, *5*, doi:10.1038/ncomms6608.

Knies, J., et al. (2014b), Effect of early Pliocene uplift on late Pliocene cooling in the Arctic-Atlantic gateway, *Earth Planet. Sci. Lett.*, *387*, 132–144.

Kozdon, R., D. C. Kelly, K. Kitajima, A. Strickland, J. H. Fournelle, and J. W. Valley (2013), In situ $\delta^{18}O$ and Mg/Ca analysis of diagenetic and planktic foraminiferal calcite preserved in a deep-sea record of the Paleocene-Eocene thermal maximum, *Paleoceanography*, *28*, 517–528, doi:10.1002/palo.20048.

Laskar, J., P. Robutel, F. Joutel, M. Gastineau, A. C. M. Correia, and B. Levrard (2004), A long-term numerical solution for the insolation quantities of the Earth, *Astron. Astrophys.*, *428*(1), 261–285.
Lawrence, K. T., T. D. Herbert, C. W. Brown, M. Raymo, and A. M. Haywood (2009), High-amplitude variations in North Atlantic sea surface temperature during the early Pliocene warm period, *Paleoceanography*, *24*, PA2218, doi:10.1029/2008PA001669.
Lisiecki, L. E., and M. E. Raymo (2005), A Pliocene-Pleistocene stack of 57 globally distributed benthic $\delta^{18}O$ records, *Paleoceanography*, *20*, PA1003, doi:10.1029/2004PA001071.
Lunt, D. J., P. J. Valdes, A. Haywood, and I. C. Rutt (2008), Closure of the Panama Seaway during the Pliocene: Implications for climate and Northern Hemisphere glaciation, *Clim. Dyn.*, *30*, 1–18.
Martínez-Botí, M. A., G. L. Foster, T. B. Chalk, E. J. Rohling, P. F. Sexton, D. J. Lunt, R. D. Pancost, M. P. S. Badger, and D. N. Schmidt (2015), Plio-Pleistocene climate sensitivity evaluated using high-resolution CO_2 records, *Nature*, *518*, 219–222.
Matthiessen, J., J. Knies, C. Vogt, and R. Stein (2009), Pliocene paleoceanography of the Arctic Ocean and subarctic seas, *Philos. Trans. R. Soc. London, Ser. A*, *367*, 21–48.
Mauritzen, C. (1996), Production of dense overflow waters feeding the North Atlantic across the Greenland-Scotland Ridge. Part 1: Evidence for a revised circulation scheme, *Deep Sea Res., Part I*, *43*, 769–837.
Mestas-Nunez, A. M., and P. Molnar (2014), A mechanism for freshening the Caribbean Sea in pre-Ice Age time, *Paleoceanography*, *29*, 508–517, doi:10.1002/2013PA002515.
Miller, G. H., R. B. Alley, J. Brigham-Grette, J. J. Fitzpatrick, L. Polyak, M. C. Serreze, and J. W. C. White (2010), Arctic amplification: Can the past constrain the future?, *Quat. Sci. Rev.*, *29*, 1779–1790.
Miller, K. G., J. D. Wright, J. V. Browning, A. Kulpecz, M. Kominz, T. R. Naish, B. S. Cramer, Y. Rosenthal, W. R. Peltier, and S. Sosdian (2012), High tide of the warm Pliocene: Implications of global sea level for Antarctic deglaciation, *Geology*, *40*(5), 407–410.
Mudelsee, M., and M. E. Raymo (2005), Slow dynamics of the Northern Hemisphere glaciation, *Paleoceanography*, *20*, PA4022, doi:10.1029/2005PA001153.
Müller-Michaelis, A., G. Uenzelmann-Neben, and R. Stein (2013), A revised Early Miocene age for the instigation of the Eirik Drift, offshore southern Greenland: Evidence from high-resolution seismic reflection data, *Mar. Geol.*, *340*, 1–15.
Orvik, K. A., and P. Niiler (2002), Major pathways of Atlantic water in the northern North Atlantic and Nordic Seas towards Arctic, *Geophys. Res. Lett.*, *29*(19), 1896, doi:10.1029/2002GL015002.
Otterå, O. H., and H. Drange (2004), A possible feedback mechanism involving the Arctic freshwater, the Arctic sea ice, and the North Atlantic drift, *Adv. Atmos. Sci.*, *21*(5), 784–801.
Pagani, M., Z. Liu, J. LaRiviera, and A. C. Ravelo (2010), High Earth-system climate sensitivity determined from Pliocene carbon dioxide concentrations, *Nat. Geosci.*, *3*, 27–30.
Panitz, S., U. Salzmann, B. Risebrobakken, S. De Schepper, and J. M. Pound (2016), Climate variability and long-term expansion of peat lands in Arctic Norway during the late Pliocene (ODP Site 642, Norwegian Sea), *Clim. Past*, *12*, 1043–1060, doi:10.5194/cp-12-1043-2016.
Pearson, P. N., and C. E. Burgess (2008), Foraminifer test preservation and diagenesis: Comparison of high latitude Eocene sites, in *Biogeochemical Controls on Paleoceanographic Environmental Proxies*, edited by W. E. N. Austin and R. H. James, pp. 59–72, Geol. Soc., London.
Pearson, P. N., and M. R. Palmer (2000), Atmospheric carbon dioxide concentrations over the past 60 million years, *Nature*, *406*, 695–699.
Pearson, P. N., P. W. Ditchfield, J. Singano, K. G. Harcourt-Brown, C. J. Nicholas, R. K. Olsson, N. J. Shackleton, and M. A. Hall (2001), Warm tropical sea surface temperatures in the Late Cretaceous and Eocene epochs, *Nature*, *413*, 481–487.
Poore, H. R., R. Samworth, N. J. White, S. M. Jones, and I. N. McCave (2006), Neogene overflow of Northern Component Water at the Greenland-Scotland Ridge, *Geochem. Geophys. Geosyst.*, *7*, Q06010, doi:10.01029/02005gc001085.
Poore, R. Z., and W. A. Berggren (1975), The morphology and classification of Neogloboquadrina atlantica (Berggren), *J. Foraminif. Res.*, *5*(2), 76–84.
Ravelo, A. C., and C. Hillaire-Marcel (2007), The use of oxygen and carbon isotopes of foraminifera in paleoceanography, in *Proxies in Late Cenozoic Paleoceanography*, edited by C. Hillaire-Marcel and A. de Vernal, pp. 735–764, Elsivier, Neth.
Raymo, M. E., J. X. Mitrovica, M. J. O'Leary, R. M. DeConto, and P. J. Hearty (2011), Departure from eustasy in Pliocene sea-level records, *Nat. Geosci.*, *4*(5), 328–332.
Risebrobakken, B., E. Jansen, C. Andersson, E. Mjelde, and K. Hevrøy (2003), A high-resolution study of Holocene paleoclimatic and paleoceanographic changes in the Nordic Seas, *Paleoceanography*, *18*(1), 1017, doi:10.1029/2002PA000764.
Risebrobakken, B., T. Dokken, L. H. Smedsrud, C. Andersson, E. Jansen, M. Moros, and E. V. Ivanova (2011), Early Holocene temperature variability in the Nordic Seas: The role of oceanic heat advection versus changes in orbital forcing, *Paleoceanography*, *26*, PA4206, doi:10.1029/2011PA002117.
Robinson, M. M. (2009), New quantitative evidence of extreme warmth in the Pliocene Arctic, *Stratigraphy*, *6*(4), 265–275.
Robinson, M. M., P. J. Valdes, A. M. Haywood, H. J. Dowsett, D. J. Hill, and S. M. Jones (2011), Bathymetric controls on Pliocene North Atlantic and Arctic sea surface temperature and deepwater production, *Paleogeogr. Paleoclimatol. Paleoecol.*, doi:10.1016/j.palaeo.2011.1001.1004.
Rühlemann, C., S. Mulitza, P. J. Müller, G. Wefer, and R. Zahn (1999), Warming of the tropical Atlantic Ocean and slowdown of thermohaline circulation during the last deglaciation, *Nature*, *402*, 511–514.
Sarnthein, M., G. Bartoli, M. Prange, A. Schmittner, B. Schneider, M. Weinelt, N. Andersen, and D. Garbe-Schonberg (2009), Mid-Pliocene shifts in ocean overturning circulation and the onset of Quaternary-style climates, *Clim. Past*, *5*(2), 269–283.
Schreck, M., M. Meheust, R. Stein, and J. Matthiessen (2013), Response of marine palynomorphs to Neogene climate cooling in the Iceland Sea (ODP Hole 907A), *Mar. Micropaleontol.*, *101*, 49–67.
Seki, O., G. L. Foster, D. N. Schmidt, A. Mackensen, K. Kawamura, and R. D. Pancrost (2010), Alkenone and boron-based Pliocene pCO_2 records, *Earth Planet. Sci. Lett.*, *292*, 201–211.
Sexton, P. F., P. A. Wilson, and P. N. Pearson (2006), Microstructural and geochemical perspectives on planktic foraminiferal preservation: "Glassy" versus "Frosty", *Geochem. Geophys. Geosyst.*, *7*, Q12P19, doi:10.1029/2006GC001291.
Shipboard Scientific Party (1987), Site 644, in *Proc. Init. Repts. (Pt. A)*, vol. 104, edited by O. Eldholm et al., pp. 617–751, ODP, Washington, D. C.
Short, D. A., J. G. Mengel, T. J. Crowley, W. T. Hyde, and G. R. Norths (1991), Filtering of Milankovitch cycles by Earth's geography, *Quat. Res.*, *35*, 157–173.
Smedsrud, L. H., et al. (2013), The role of the Barents Sea in the Arctic climate system, *Rev. Geophys.*, *51*, 415–449, doi:10.1002/Rog.20017.
Spiegler, D., and E. Jansen (1989), Planktonic foraminifer biostratigraphy of Norwegian Sea sediments: ODP Leg 104, in *Proceedings of the Ocean Drilling Program, Scientific Results, 104*, edited by O. Eldholm et al., pp. 681–696, Ocean Drilling Program, College Station, Tex.

Stap, L. B., B. de Boer, M. Ziegler, R. Bintanja, L. J. Lourens, and R. S. W. van de Wal (2016), CO_2 over the past 5 million years: Continuous simulation and new δ^{11}B-based proxy data, *Earth Planet. Sci. Lett.*, *439*, 1–10.

Verhoeven, K., S. Louwye, J. Eiríksson, and S. De Schepper (2011), A new age model for the Pliocene-Pleistocene Tjörnes section on Iceland: Its implication for the timing of North Atlantic-Pacific paleoceanographic pathways, *Paleogeogr. Paleoclimatol. Paleoecol.*, *309*, 33–52.

Voigt, J., E. C. Hathorne, M. Frank, and A. Holbourn (2016), Minimal influence of recrystallization on middle Miocene benthic foraminiferal stable isotope stratigraphy in the eastern equatorial Pacific, *Paleoceanography*, *31*, 98–114, doi:10.1002/2015PA002822.

Williams, M., A. M. Haywood, C. D. Hillenbrand, and I. P. Wilkinson (2005), Efficacy of δ^{18}O data from Pliocene planktonic foraminifer calcite for spatial sea surface temperature reconstruction: Comparison with a fully coupled ocean-atmosphere GCM and fossil assemblage data for the mid-Pliocene, *Geol. Magazine*, *142*, 399–417.

Zachos, J. C., B. P. Flower, and H. Paul (1997), Orbitally paced climate oscillations across the Oligocene/Miocene boundary, *Nature*, *388*, 567–570.

Zachos, J. C., G. R. Dickens, and R. E. Zeebe (2008), An early Cenozoic perspective on greenhouse warming and carbon-cycle dynamics, *Nature*, *451*, 279–283.